THE DEVELOPMENT OF AN ORE PASS LEVEL INDICATOR

Gary M. Rix

BSc(Eng). Cape Town

University of Cape Town

Thesis submitted to the Department Of Electrical and Electronic Engineering of the University of Cape Town in partial fulfilment of the requirements for the Degree MSc(Eng).

The University of Cape Town has been given the right to reproduce this thesis in whole or in part. Copyright is held by the author.

The copyright of this thesis vests in the author. No quotation from it or information derived from it is to be published without full acknowledgement of the source. The thesis is to be used for private study or non-commercial research purposes only.

Published by the University of Cape Town (UCT) in terms of the non-exclusive license granted to UCT by the author.

University of Cape Town

DECLARATION.

I declare that this dissertation is my own unaided work. It is being submitted in partial fulfilment of the requirements for the degree of Master of Science in Engineering at the University of Cape Town. It has not been submitted before for any degree or examination at any other university.

Signed by candidate

26 day of April 1990.

ABSTRACT.

All open cast mines have a limited economic life which is usually dictated by the so called economic depth, where the costs of hauling the ore via large diesel trucks becomes prohibitive. A mine that is about to reach its economic depth is the Finsch mine. In order to prolong its life mining will now take place underground [1.1]. Ore passes, vertical storage shafts, will form the backbone of the new mine. Safe and efficient mining calls for the depth of ore in these ore passes to be monitored accurately [1.2].

This thesis is concerned with the design and construction of such an instrument. The ore pass could in theory propagate a number of waveguide modes. However, with the particular frequency chosen for the instrument reported here, the mode of propagation was the same mode as free-space. A FMCW radar system was designed for this specific application but had the advantage that testing could take place in free-space. Two prototype systems were constructed and tested down the ore pass which proved the instrument concept satisfactorily. The instrument has definite commercial viability.

ACKNOWLEDGEMENTS.

The author would like to thank Professor B.J. Downing for his guidance and support during this project.

The author would like to thank De Beers Diamond Research Laboratories for their financial support and assistance. In particular, thanks are due to Dr. D. Salter., the staff of the Finsch mine and Mr. M.G. Marais (Finsch Mine engineer) for tolerating the long hours, trying conditions and making the systems tests possible. The other members of the De Beers Research team for being themselves.

The technical and social support of fellow students and staff was greatly appreciated, in particular Mr. S. Schrire, Chief Technical Officer.

The financial assistance from the Council for Scientific and Industrial Research was greatly appreciated.

TABLE OF CONTENTS.

LIST OF ILLUSTRATIONS.

FIGURES.

TABLES.

Chapter 1
INTRODUCTION.

Diamond mining is generally done by means of an open-cast or pit mining technique. A hole is made following the contours of the kimberlite or diamond-bearing rock. The rock is removed in a series of steps or open-pit benches usually by means of explosives.

The ore is then transported to the surface processing plant by means of large diesel trucks, that travel up spiral track which is built into the side-wall of the pit. However as the pit grows deeper, the length of the spiral track increases and production costs escalate. The pit is then said to have reached its economic depth.[1.1]

Figure 1.1. Finsch treatment plant with openpit mine in background.

The Finsch diamond Mine, located 160 km north-west of Kimberly in the Northern Cape will reach its economic depth in 1990, at a depth of 390m below the surface. This mine has been operated by the De Beers Consolidated Mine Ltd since 1963 and processes approximately 5.8 Megatonnes of ore to yield approximately 5.0 Megacarats of diamonds a year. Sixty five to seventy percent of these diamonds are of industrial quality.

Various means have been devised to extend the lives of these so called uneconomic mines. One of these newer techniques is to move the mining operations underground [1.1], this technique is been implemented at the Finsch Mine. A network of tunnels is constructed around the kimberlite ore and the ore is removed, by standard mining techniques, in a series of horizontal or production shafts which extend into the kimberlite pipe as shown in Fig. 1.2 and Fig. 1.3.

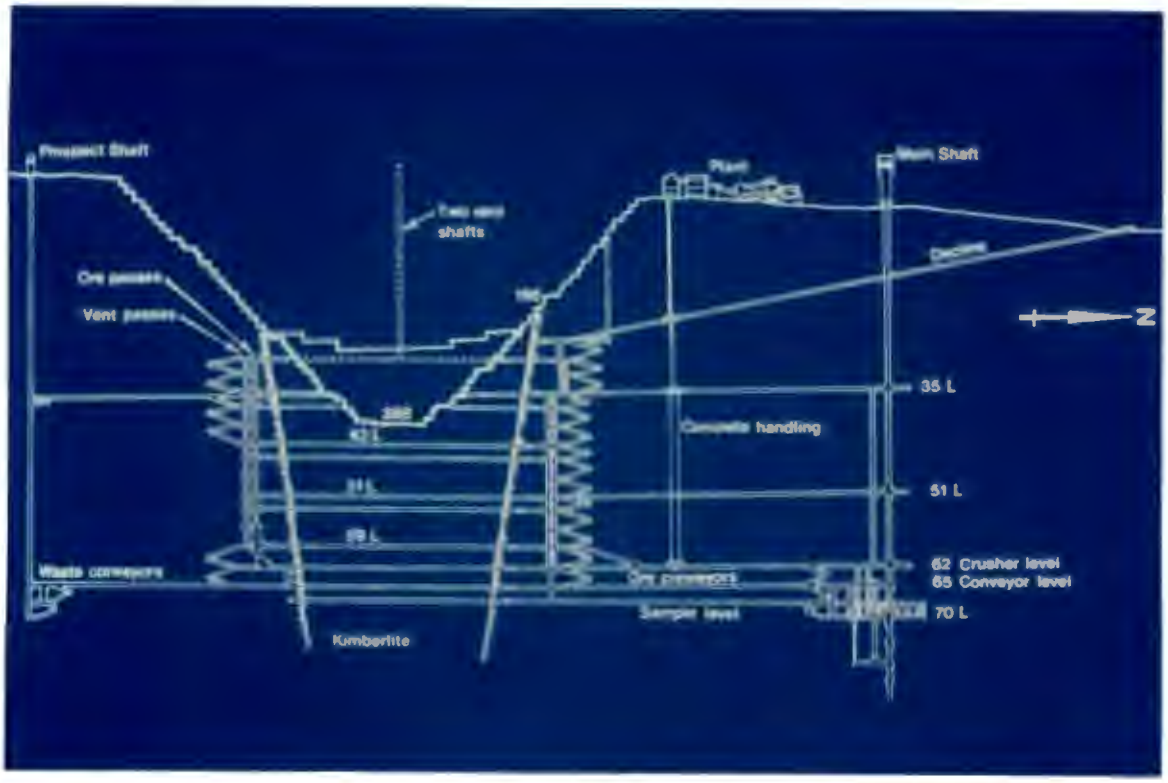

Figure 1.2. Diagrammatic section of Finsch diamond mine.

Around the kimberlite pipe, vertical shafts are sunk from below the economic depth to a crushing level situated deeper down. The shafts are used to convey the ore from the production level to

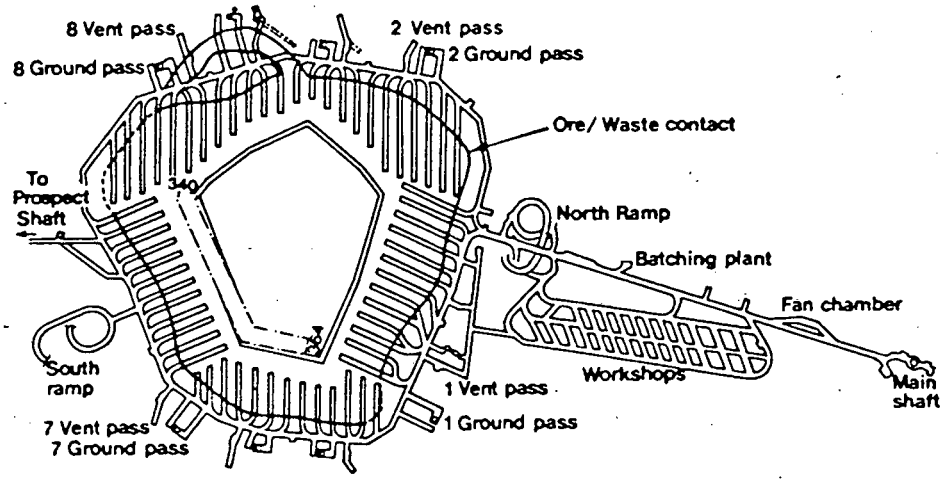

Figure 1.3. Layout of 35m underground level.

the crushing level, under the action of gravity, and are called ore or ground passes as shown in Fig. 1.4.

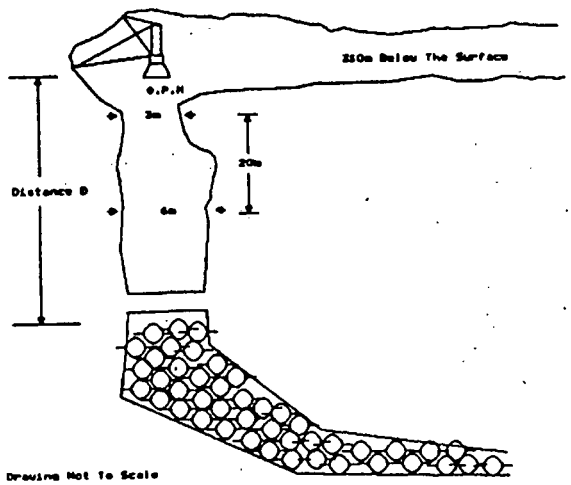

Figure 1.4. Diagrammatic of ore pass monitor location.

At the crushing station the ore is reduced in particle size to a more manageable size. It is then transported by means of skips or ore lifts to the surface processing plant. From where processing of the ore continues as for a normal open-cast mine.

The object of this study is to determine whether a technique for the monitoring of the level of ore in the ore passes can be developed. The knowledge of the ore level is important as the shaft must never be allowed to become empty. This condition will allow the falling ore to have access to the crushing station equipment and operators. A small amount of ore will have to be retained at the bottom of the ore pass to act as a shock absorber for the falling rocks. To act as a safety back-up the equipment developed on this project will work in conjunction with a low-level alarm, which itself has many safety features built-in.

The ore pass was not completed when this study commenced and local test sites or tunnels do not exist. The lack of relevant data or research in this area was limited to a few papers none dealt with their data in a practical form. Thus use was made of a small local test-site and the assumption that scaling of results would be valid until tests could be performed on the ore pass itself.

The ore passes are shafts hewn out of the solid rock body surrounding the kimberlite pipe. They extend from the primary production level, at 350 m below the surface, to the crushing station at 620 m below the surface. Thus the ore pass is 270 m deep with a roughly circular cross-section of 6 m diameter.

Table 1.1.

Table of Specifications	
Measurement update time	60 s
Maximum measurable range (shaft empty)	330 m
Minimum measurable range (shaft full)	50 m
Accuracy	5 m
Resolution	5 m

The system must be able non intrusive and satisfy the above specification. The rugged mining environment renders most level detection schemes inoperable. An optical system would require some form of reflector which could become contaminated in the dusty environment. The rocks would not be reliable optical reflectors. An acoustical ultrasonic system would require a high power to overcome the long range as well as the high background noise levels due to normal mining operations.

The constraint of non-intrusion eliminated a number of possible mechanical systems.

The system must also be able to cope with a rough wall surface, as the ore pass is constructed with explosives and the falling rocks wash the walls. It must also be able to measure as rocks are falling down the ore pass, introduced at the tipping point. The ore passes are not continuous and on each level there is a large open area which are ore tipping points as shown in Fig. 1.4.

The ore pass level indicator must also communicate with surface control computers which are responsible via PLC's for most of the process control of the underground

machinery. A microwave radar system proved to be the best solution for satisfying the above criteria.

1.0. References.

[1.1] BIRD,D. Finsch Mine. *Mining Mag.* , February 1987, 120-125.

[1.2] RIX, G., DOWNING, B.J and SALTER, J.D. Development of a Novel Ore Pass Level Indicator for Underground Mines. Proc. SAIEE. Second Joint Symp. on Antennas and Propgation and Microwave Theory and Techniques, Pretoria, South Africa.

Chapter 2
PROPAGATION CHARACTERISATION OF AN ORE PASS.

2.0. Introduction.

The attenuation of a signal is the path-loss or strength reduction that a signal experiences as it propagates through a medium. Hence the amount of attenuation that a signal experiences along a particular path is vitally important for the design of a piece of equipment that will use this path.

To minimise costs and the design complexity, the system must utilise a signal path that has the lowest attenuation for a given range.

It is well known that signals can propagate in tunnels [2.1, 2.3, 2.5, 2.7, 2.10, 2.21, 2.22]. However in some cases this is due to the existence of longitudinal conducting materials, which act as interconnecting links between the transmitter and the receiver. In some cases though propagation has taken place without any conductors in the tunnel [2.3, 2.5, 2.6, 2.7, 2.10, 2.21].

To show the different modes that a signal can propagate along a path, in a tunnel, and how the attenuation varies for the different modes, the simple form of the radar equation will be shown. This will be used as the basis for comparison as the signals involved operate in free-space or strictly without any guiding taking place, apparently the worst case for signal power transfer.

signal strength on the range R. If the range is doubled, the received power will decrease by a factor of 16 or -12 dB. For a single way link, (2.2) yields a 6 dB increase in attenuation for a doubling of distance. This form of loss is known as propagation or dispersion loss and is due to the wavefront of the signal spreading outwards as it propagates.

The simple form of the radar equation (2.3) is however generally optimistic, in terms of predicted range performance as it does not take account of the losses that are inherent in a radar system. Some of the parameters are statistical or random in nature and not constant, the receiver sensitivity, the σ of the target and meteorological conditions are examples of this. These give rise to a higher loss than that predicted by the simple radar equation.

2.2. Transmission Line Theory.

If the microwave energy were guided by the ore pass the propagation mechanism can be described by the transmission line theory. A section of a transmission line can be represented by the general lumped element circuit shown below in Fig. 2.1.

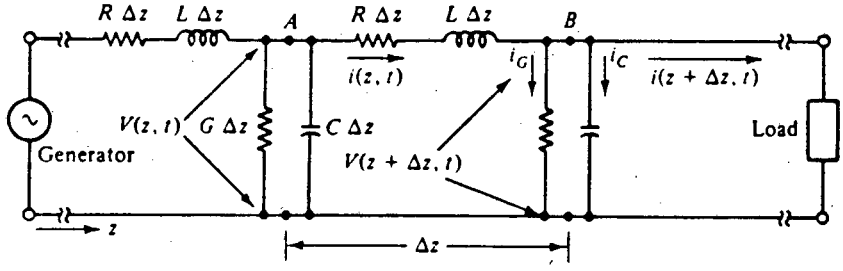

Figure 2.1. Elementary section of a transmission line.

By applying elementary circuit theory, the line or circuits response in both the time domain and the frequency domain can be calculated [2.14].

The behavior in the frequency domain is of particular importance here and the resultant equations are shown here.

$$\gamma = \sqrt{(R+jwL)(G+jwC)} \qquad (2.4)$$

The γ is known as the propagation constant and is a complex quantity,

$$\gamma = \sqrt{(\alpha+j\beta)} \qquad (2.5)$$

α is the attenuation constant [dB/m or nepers/m],
β is the phase constant [radians/m].

As mentioned earlier, the attenuation constant, α, is of importance in this study and in this case is a function of all the elementary components of the transmission line (R,G,L,C).

The total attenuation experienced by the signal along the line is proportional to the length of the link. Hence if the link length is doubled, the total attenuation measured in terms of decibels is doubled.

A transmission line, in the classical sense, is any two conductor link between two points. If the length of the line is long, compared to the physical spacing of the conductor then it can be analysed relatively easily by the methods of distributed circuit theory. It could also have been solved by the solution of Maxwell's field equations, however these involve three space variables in addition to the time variable. The distributed circuit method only

involves one space variable and the time variable and so is the preferred method of solution.

2.3. Microwave Waveguide Theory.

In general, a waveguide consists of a rectangular or a circular hollow metallic tube that is used to guide electromagnetic waves in the form of waveguide modes. Physical sizes of waveguides limits their use to the microwave range of frequencies.

When an electromagnetic wave propagates along a waveguide, its electric and magnetic fields are confined to within the guide. No power is lost through radiation and as they are usually air filled, dielectric loss is negligible. A small loss, due to the heating of the side walls, however does occur.

Several modes of electromagnetic waves can propagate within a waveguide. These modes correspond to solutions of Maxwell's equations for a particular waveguide and it has a definite cut-off frequency for each of the allowed modes. If the electromagnetic signal is above cut-off, it will propagate without any significant attenuation. Signals with a frequency below the cut-off for a particular mode will be attenuated to a negligible value in a relatively short distance.

The dominant mode of a waveguide is that mode with the lowest cut-off frequency. As the tunnels and ore passes are primarily of circular cross section, this study was confined to circular waveguides.

Most texts on waveguides simplify the analysis of waveguides by assuming that they are lossless. However

this attenuation does take place and is rigorously pursued by [2.16,2.21].

The cut-off wavelengths for a circular waveguide are given by [2.16] as :

$$TM : \lambda mn = \frac{2.\pi.r}{Xmn} \qquad (2.6)$$

$$TE : \lambda mn = \frac{2.\pi.r}{Xmn'} \qquad (2.7)$$

where r = radius of the waveguide
Xmn = nth nonvanishing root of the mth order Bessel function
Xmn' = first derivative of Xmn

Below cut-off, the attenuation rate is given by [2.20] as :

$$\alpha = \frac{54.6}{\lambda c} \sqrt{\left(1 - \left(\frac{\lambda c}{\lambda}\right)^2\right)} \quad dB/m \qquad (2.8)$$

where λc = dominant mode wavelength

The attenuation rate is independent of the electrical properties of the walls of the guide. It increases as the frequency is increased towards the limiting value given by (2.8). Above cut-off the attenuation of each of the modes depends on the frequency, shape, dimensions and the electrical properties of the waveguide.

The attenuation, α, of a circular waveguide is given by [2.16] as :

$$TMmn: \quad \alpha = \frac{8.69 * R}{Zo.r} \cdot \frac{1}{\sqrt{1-(\lambda/\lambda mn)^2}} \quad dB/m \quad (2.9)$$

$$TEmn: \quad \alpha = \frac{8.69.R}{Zo.r} * \left[\frac{m^2}{((X'mn)^2 - m^2} + \left(\frac{\lambda}{\lambda mn} \right)^2 \right] \frac{1}{\sqrt{1-(\lambda/\lambda mn)}} \quad dB/m \quad (2.10)$$

where Zo = Characteristic Impedance of Medium. ($\sqrt{(\mu m/\epsilon m)}$) , σ = conductivity of wall.

$R = 10.88 * 10^{-3} * \sqrt{((10^7/\sigma)(1/\lambda))}$

Here again, the attenuation rate is constant per unit length, hence doubling the length of the waveguide leads to a doubling of the total attenuation (in dB) for a doubling of the distance.

2.4. Discussion Of The Theoretical Background.

The theoretical development shown for the waveguide case above is only applicable for highly conducting hollow guides. Even then in most cases real waveguides are considered to be lossless, which simplifies analysis, but tunnels and ore passes are far from this ideal.

Analysis of the results of Monk and Winbigler[2.18] in a railway tunnel shown in Fig 2.2 or those obtained by Ivanov, Sakalo and Puskar[2.11] in a mine tunnel Fig 2.3, waveguide behavior cannot easily be seen [2.6]. With decreasing frequency, the attenuation increases but does not reach the asymptotic value predicted by (2.8). More importantly, a distinct cut-off frequency does not appear in either Fig 2.2 or Fig 2.3 [2.6, 2.11, 2.18].

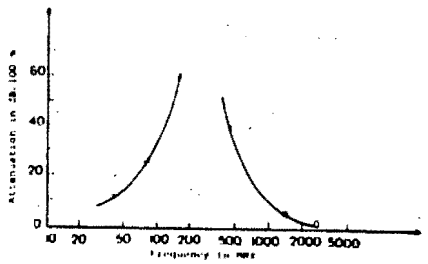

Figure 2.2. Attenuation vs Frequency in a railway tunnel [Monk & Winbigler].

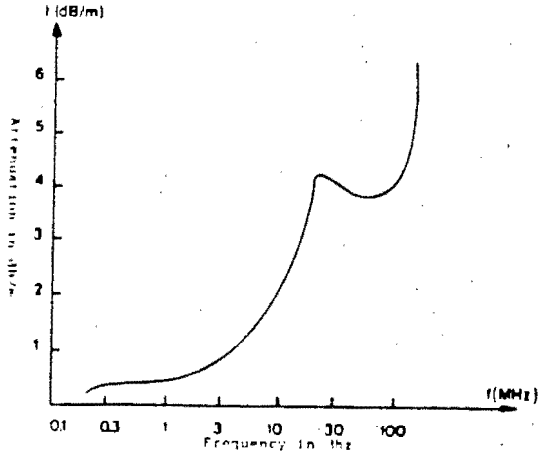

Figure 2.3. Attenuation vs Frequency in a mine tunnel [Ivanov,Sakalo & Puskar].

The major difference between a waveguide and an actual tunnel is that the conductivity of the latter is very low. This limits the waveguide model in two areas. Firstly, as frequency increases, the walls act as a dielectric medium rather than as a conducting wall. At high frequencies there is a loss due to the refraction of part of the energy into the wall, while a small amount is reflected back into the tunnel [2.6]. Mahmoud and Wait, Emslie, Lagace and Strong [2.7] used geometric optics and the ray method respectively, to show the increase in modal attenuation due to wall roughness as frequency is increased. However the total attenuation is a decreasing function of frequency, provided operation above cut-off is maintained [2.6].

The second limitation is that as the carrier frequency is reduced below cut-off, the electromagnetic wave can propagate through the rock and is not guided by the tunnel at all.

The attenuation when this occurs is given by [2.9] as

$$\alpha = 8.69 \sqrt{(2\pi f \mu \sigma / 2)} \quad \text{dB/m} \qquad (2.11)$$

Where f = frequency [Hz]
μ = permeability of rock [henry/m]
σ = conductivity of rock [mho/m]

This equation explains why a definite cut-off frequency does not always appear when field strength measurements are made in some tunnels. This occurs when attenuation due to (2.11) is lower than that due to (2.8) and the majority of the signal propagates through the rock around the tunnel [2.6].

Another reason that the results can seem anomalous can be due to spurious or unknown TEM modes propagating in the tunnel. It is well documented that TEM modes can propagate wherever there are longitudinal metallic conductors such as pipes, railway tracks etc [2.1, 2.5, 2.10,2.15].

Generally no information about the exact electrical characteristics of the tunnels are available. The characteristics that are found in tables are useless for this application, as the conductivity and permittivity are dependant on the frequency, rock anisotropy and surface moisture etc. [2.8]. The data presented in these tables usually comes from laboratory prepared samples of rock with uniform thickness and smooth surfaces.

Deryck's results for a tunnel of approximately 5 m diameter and 1600 m long in Lanaye, Belgium are shown in Fig 2.4. On this data curve, various theoretical curves are also shown, these represent the various modes that can exist in the tunnel. The cut-off frequency for this tunnel is approximately 35 MHz, TE11 mode.

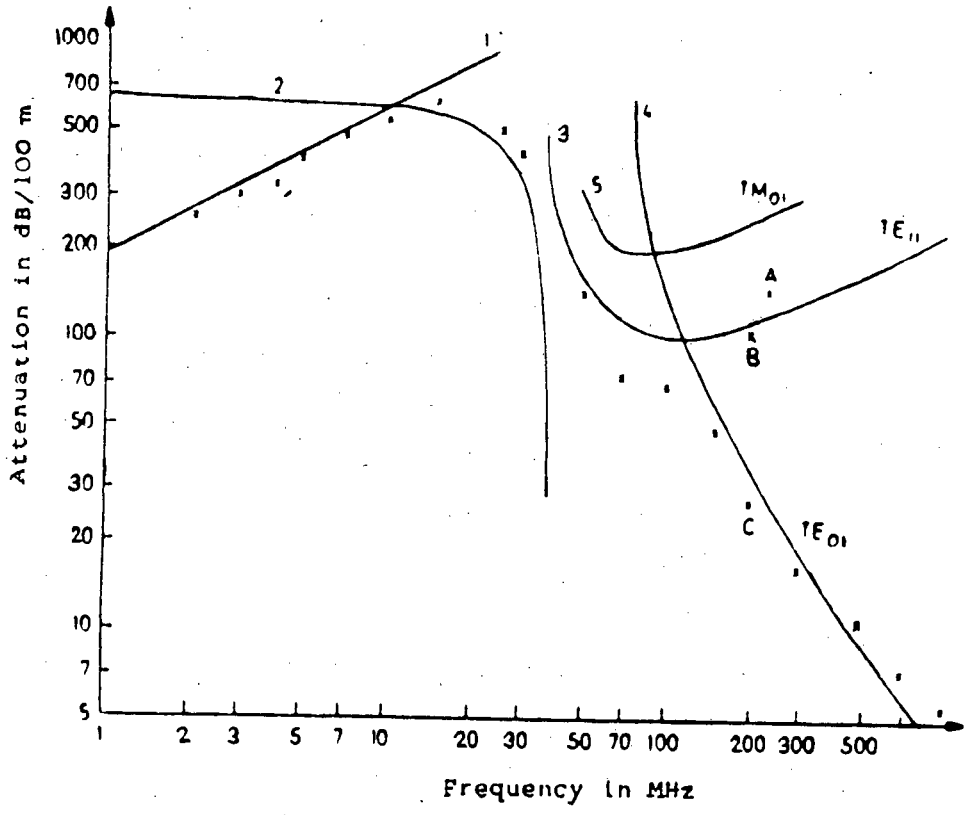

Figure 2.4. Measured and theoretical attenuation in a tunnel near Lanaye. [Deryk].

Curves 1-2: Represent propagation through a medium with a conductivity of 10 mho/m and a circular waveguide below cut-off respectively.

Curves 3-5: Are the theoretical attenuations for the TE11, TE01 and the TM11 modes respectively from (2.7) and (2.6).

These curves show that the propagation takes place via the mode that offers the lowest attenuation [2.6].

2.5. Recent Experimental Results.

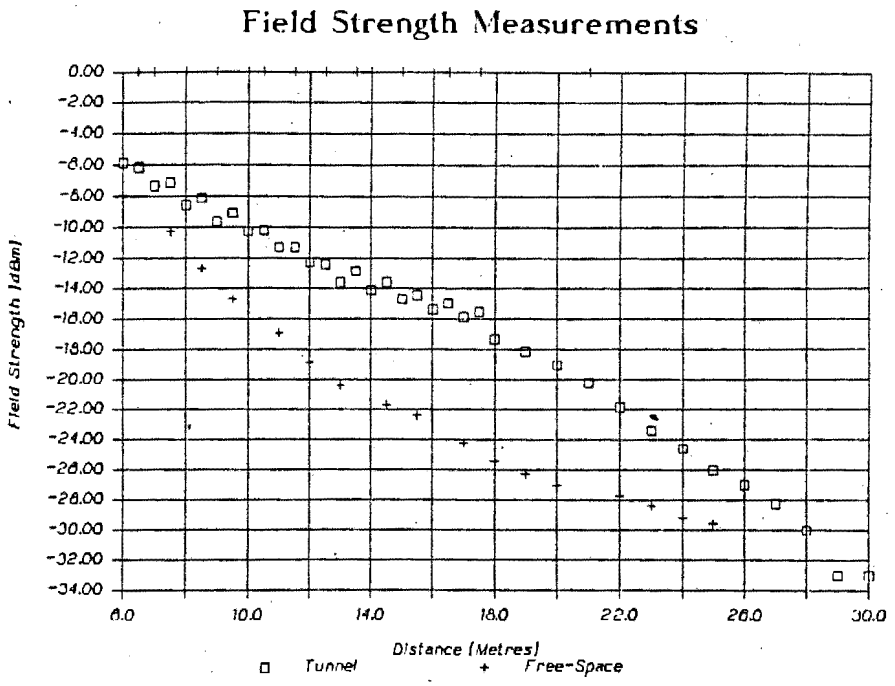

Figure 2.5. Field strength measurements in a tunnel at UCT.

Figure 2.5 shows the relative field strength measurements taken by the author at a small local test site at a frequency of 520 MHz. This tunnel is 35 m long, 1.7 m wide and 1.5 m high and of rectangular cross section. It is cement lined and the walls are smooth. Data for free space field strength measurements are also included on Fig 2.5. Figures 2.6 and 2.7 show a photograph of the test site and a diagrammatic of the test equipment used for the experiment respectively.

Figure 2.6. Photograph of the local test-site.

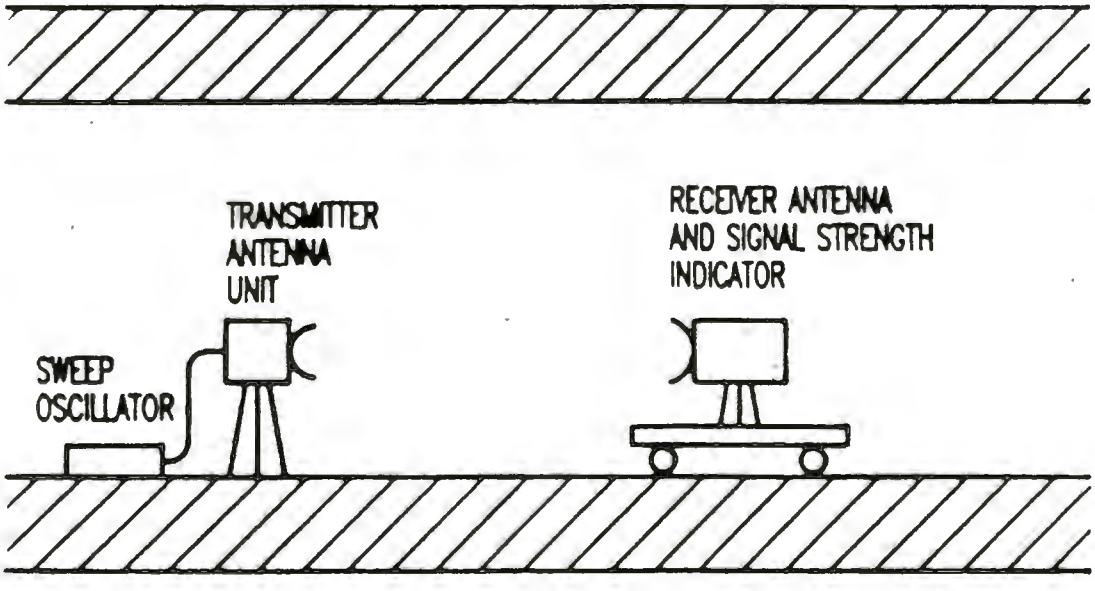

Figure 2.7. UHF/Microwave tunnel test equipment.

Similar tests were performed over a range of frequencies to ascertain the wide band response of the tunnel. The results from the tests over the frequency 137 MHz to 8.6 GHz is shown in Table 2.1. and in graphical form in Fig 2.8. Attenuation rates at lower frequencies are high where operation is around the cut-off frequency for the tunnel.

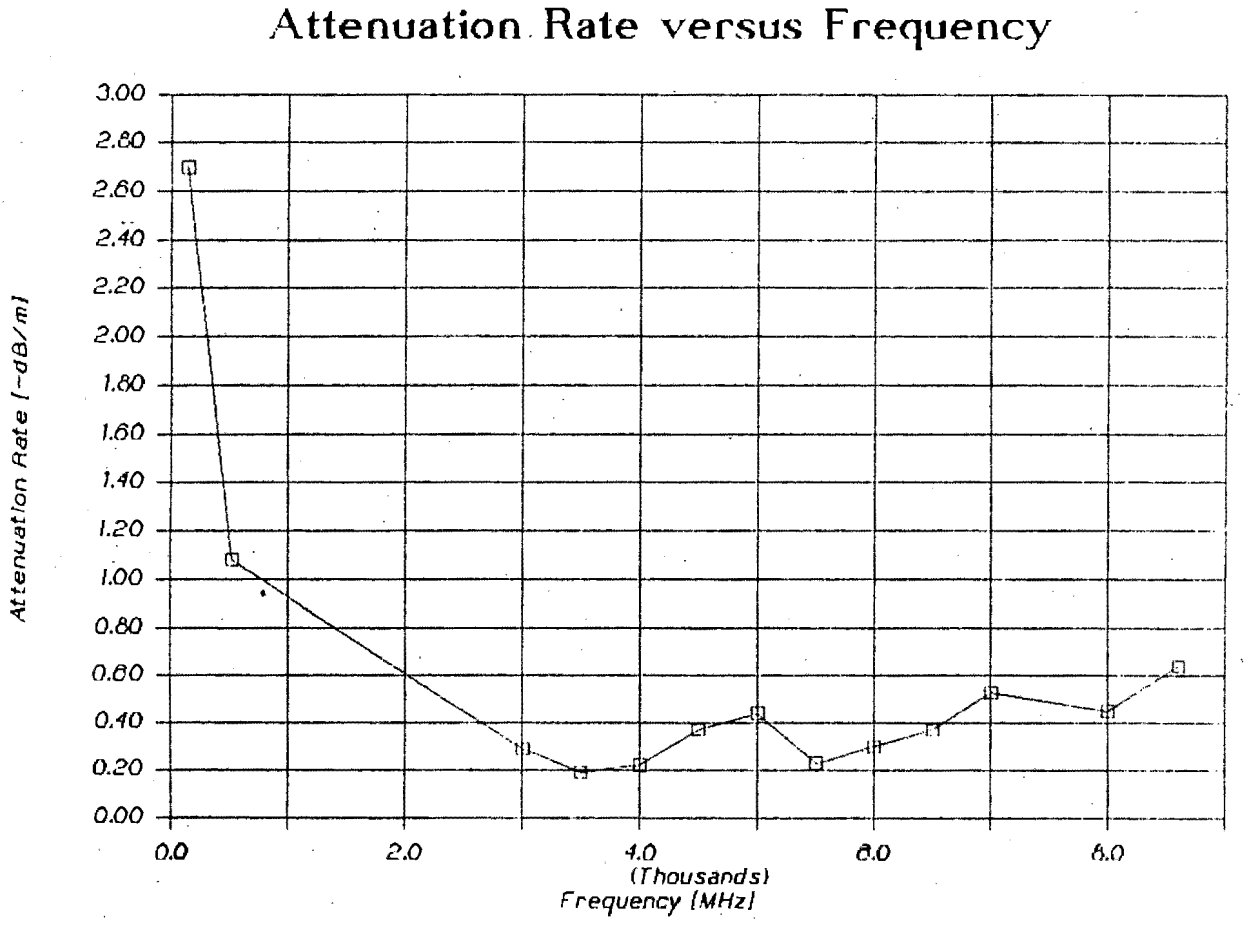

Figure 2.8. Wide band attenuation rates vs frequency for the local test site.

Table 2.1.

Wideband Attenuation Rates Vs Frequency for local test site.	
Frequency [MHz]	Attenuation [dB/m]
137	-2.70
520	-1.08
3000	-0.28
3500	-0.19
4000	-0.22
4500	-0.37
5000	-0.44
5500	-0.23
6000	-0.30
6500	-0.37
7000	-0.53
8000	-0.45
8600	-0.64

As the frequency increases, the attenuation rate decreases effectively plateauing, reaching an asymptotic value. Increasing the frequency causes the waveguide/tunnel to become increasingly overmoded. This means that the tunnel dimensions become larger when measured in terms of the wavelength of the signal propagating in the waveguide.

It is well known that overmoding a waveguide, particularly a circular waveguide, leads to a large reduction of the attenuation rate [2.13].

2.6. Low Loss Propagation.

The TE01 mode in circular waveguide is one of the higher order circularly symmetric modes that specifically has a much reduced attenuation rate. As total attenuation is a primary design consideration, identification of the mode with the lowest attenuation rate is paramount for the success of the project or will be helpful in the simplification of the final unit.

Figure 2.9 shows the different field distributions for circular waveguides, while Fig 2.10 shows typical attenuation rates for the different modes in smooth conducting wall waveguides.

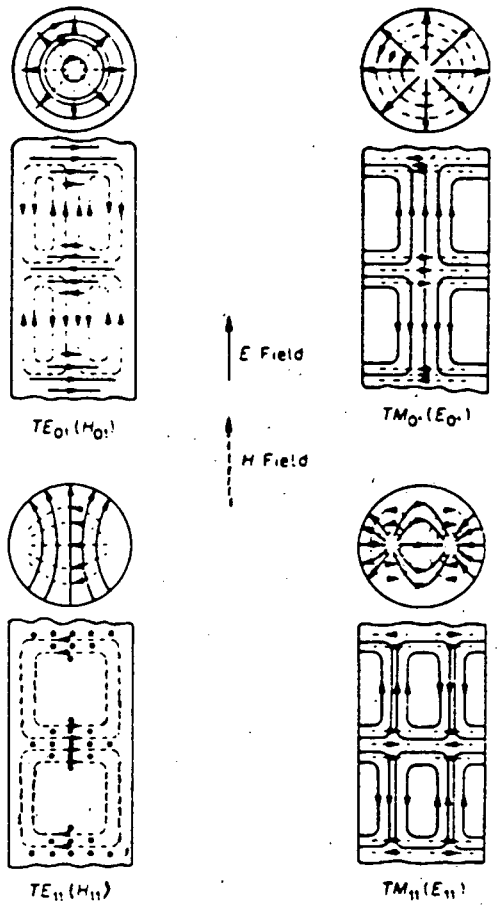

Figure 2.9. Field distributions for different modes in circular waveguide.

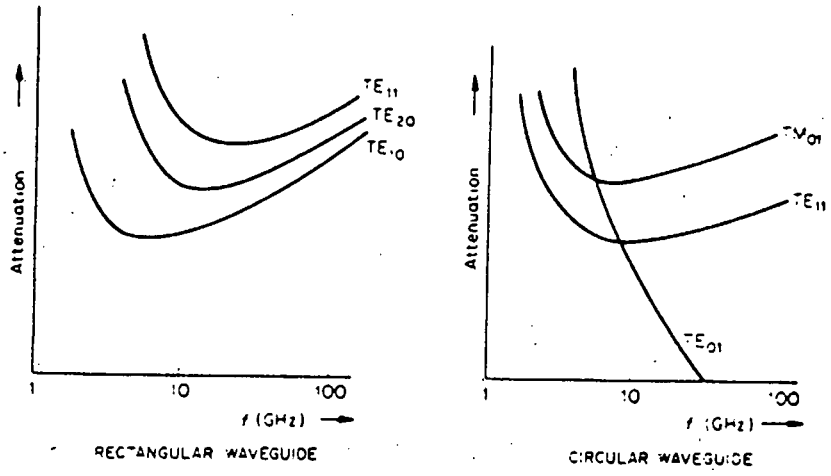

Figure 2.10. Typical attenuation rates for different modes in circular and rectangular waveguide.

The TE01 mode clearly has a monotonically decreasing attenuation rate with increasing frequency. All other non-circularly symmetric modes exhibit a minimum in their attenuation curves which usually occurs just above the cut-off frequency for that mode. The attenuation rate of all modes can be reduced by increasing the cross sectional dimensions of any circular or rectangular waveguide.

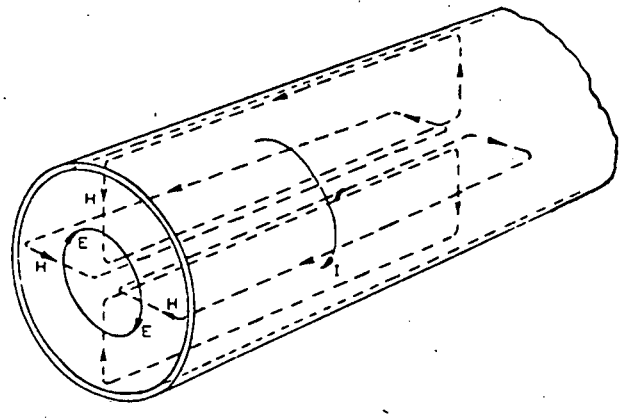

Figure 2.11. E & H Fields of the H01 mode. (TE01 Circular mode.)

The H-lines of the TE01 mode form loops in radial planes and are uniformly distributed in the circumferential direction. The E-lines form a series of closed concentric circles, with a maximum intensity at half the radius of the guide as shown in Fig 2.11. The E-field is zero at the center of the guide as well as at the waveguide walls (in the absence of losses). Due to the E-field there are circumferential currents which flow in the waveguide wall. Because of the finite conductivity of the walls, this results in power being dissipated in the form of I^2R losses, which is the attenuation mechanism [2.13].

Low loss propagation can, therefore, be associated with low wall currents. The loss is proportional to the square of the magnitude of the wall current which is in turn proportional to the intensity of the magnetic field tangential to the side walls. The magnetic field intensity decreases with the square of the cross sectional dimensions. While the periphery of the waveguide only increases linearly, the loss must therefore decrease with an increase in the size of the waveguide [2.13].

The major disadvantage of this mode is that the waveguide is highly overmoded and it thus means that it is able to propagate many unwanted modes.

Unfortunately the TE01 mode is very sensitive to the straightness of the waveguide as well as surface irregularities. Any small kink, dent or ellipticity scatters a small amount of the incident microwave energy, essentially coupling it out of the low loss mode. Further in the case of the ore pass energy will be converted due to free falling rocks. The percentage power coupled out in this way is constant irrespective of power level and has the effect of increasing the effective attenuation rate. The

possibility of mode reconversion also exists where energy in an unwanted mode can be reconverted back into the TE01 mode.

Avoiding mode conversion in practical runs of waveguides is virtually impossible as no guide can be perfectly circular, exactly straight and have a uniform cross section over its whole length.

Calculations show that an elliptical length of waveguide will have a much higher attenuation rate than a similarly sized circular waveguide [2.4].

Measurements on a different sized waveguides over a range of frequencies show that the attenuation of the TE01 mode is critically dependant on the surface resistivity and the ellipticity of the waveguide as the theory predicts. The attenuation of small waveguides is closer to the theoretical as the waveguide maintains its trueness after manufacture and during handling. The larger waveguides tend to have an elliptical cross section due to easier deformation taking place and as a result the attenuation rate is higher [2.2].

However measured attenuation for sections of waveguides that have randomly oriented sections of elliptical cross section are lower than that predicted by the theory for elliptical waveguides. Deformed waveguides can thus be used provided the deformations are not all in the same plane. Thus the attenuation will not be as low as for circular waveguide [2.2].

In conducting waveguides, the primary loss is due to mode conversion as the dielectric loss is low (for air filled waveguides). The surface loss of the walls is low due to the high conductivity of the walls.

Analytically the attenuation, in a circular waveguide of radius ro, is given by the following equation [2.2].

$$\alpha = \frac{Rs}{Zo}\left\{\frac{(fc/f)^2}{ro\sqrt{(1-(fc/f)^2)}}\right\} \text{ neper/m} \qquad (2.12)$$

Where fc = cutoff frequency
f = frequency of propagation
Rs = Surface resistance of the wall

$$= \frac{\pi f \mu m}{\sigma} \qquad (2.13)$$

μm = permeability of wall
σ = conductivity of wall
Zo = Characteristic impedance of dielectric within the waveguide.

Investigation of equation (2.12) gives the conditions of low loss propagation as.

i) ro large and the ratio (fc/f) small ie overmoding of the waveguide.
ii) Have a small surface resistance component ie Rs small and hence a large σ (mho/m)
iii) Have as large a Zo in the waveguide, usually an air dielectric in which case Zo = 377 ohms.

The equation can be simplified (using condition (iii))

$$\alpha = \frac{152.86}{\{[ro^3.\mu.(f/fc)[(f/fc)^2-1]\}} \text{ dB/m} \qquad (2.14)$$

Measured results indicate that the conductivity of the wall is of less importance than the surface irregularities and roughness as far as attenuation is concerned [2.2].

2.6.1. Mode transducers.

Launching of the low loss mode is difficult as this process must minimise the excitation of any of the other modes that can propagate in the guide.

Excitation of the TE01 mode is usually achieved by means of a specifically designed mode converter or transducer. These devices are designed to generate the required electromagnetic field within the waveguide with the minimum of loss and the maximum bandwidth or a compromise depending which is the most important criterion.

One transducer that has relative mechanical simplicity and reasonably good performance over a limited bandwidth is shown below in Figures 2.12. and 2.13 combined.

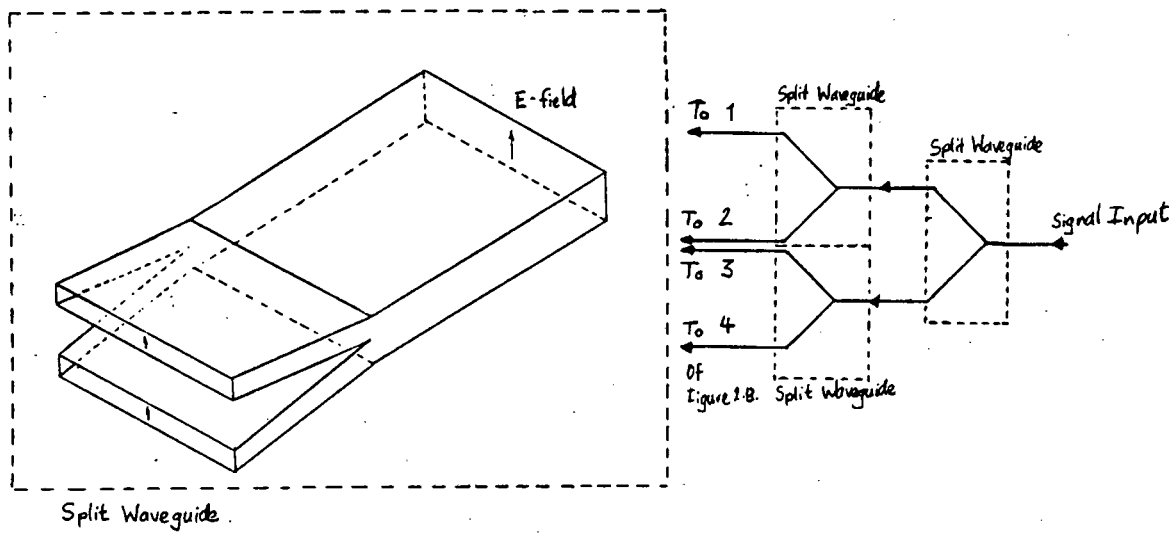

Figure 2.12. Elements of TE01 rectangular to TE01 circular mode converter.

This is achieved by splitting the rectangular feed guide (TE01 rect) in two in the E-plane. Each of these is then split in two in the E-plane as well. In other words two more of the elements shown in Figure 2.12 are connected to the outputs, yielding four outputs. This gives four waveguides as shown in Fig 2.12 , each of these can then be fed into the end of a circular waveguide. They can also be coupled through holes in the wall of the circular waveguide. The latter is the better option as it does not excite any longitudinal electric field components and is shown in Figure 2.13. More importantly, adjustable pistons can be added in each of the feeds to adjust the relative phase of each of the components. The former would require different lengths of waveguide or twisted sections of waveguide to achieve correct phasing of the components [2.2].

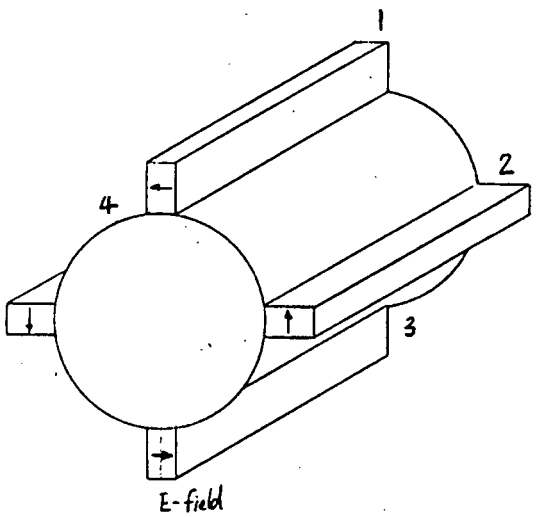

Figure 2.13. Four waveguide to TE01 circular mode converter.

The signals are launched into a circular guide that is only just able to support the TE01 mode which is then tapered out to the normal guide size.

Another transducer that has a very high efficiency and was used extensively by Karbowiak for making attenuation measurements on lengths of waveguide is shown in Fig 2.14. The input comes from a single mode rectangular waveguide which then flares out to a triangular cross section guide. This is gradually opened out to form a completely circular waveguide. Using one of these couplers and a mode filter (shown later) a transducer with a conversion loss of 0.5 dB and a 40 dB suppression of spurious modes is feasible [2.17].

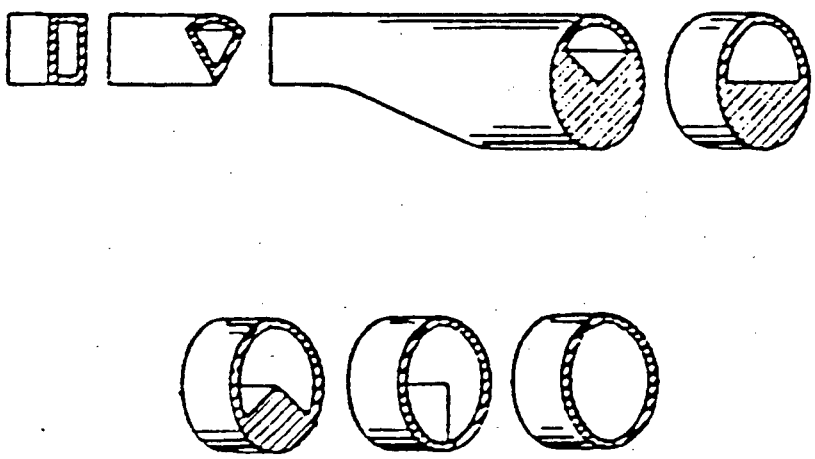

Figure 2.14. TE10 rectangular to TE01 circular mode transducer.

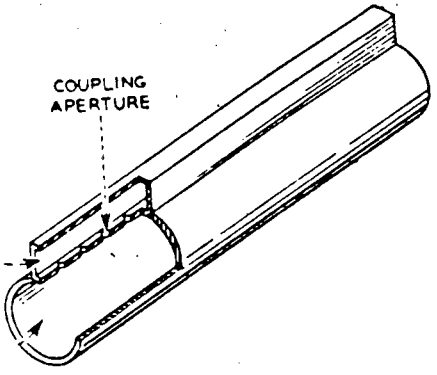

Figure 2.15. Velocity coupler for TE10 rectangular to TE01 circular mode conversion.

The velocity coupler is shown in Fig 2.15 and consists of a pair of coupled waveguides. The dimensions of the auxiliary waveguide are chosen so that the velocity of the dominant TE01 mode is equal to the velocity of the required circular waveguide mode. The power transfer is primarily in the required mode, however due to the broadband nature of the circular waveguide other modes can be excited. But by choosing a slowly varying coupling, over a long region, a substantially pure mode can be launched. This transducer is usually in the region from 0.5 to 20 wavelengths long. A transducer of the above type with a transfer loss of between 0.2 to 0.75 dB was constructed by Barlow [2.2].

2.6.2. Mode filters.

Mode filters are designed to selectively attenuate certain modes while allowing others to pass through unattenuated. Figure 2.16 shows a number of the devices used by Barlow [2.2] for his investigative work.

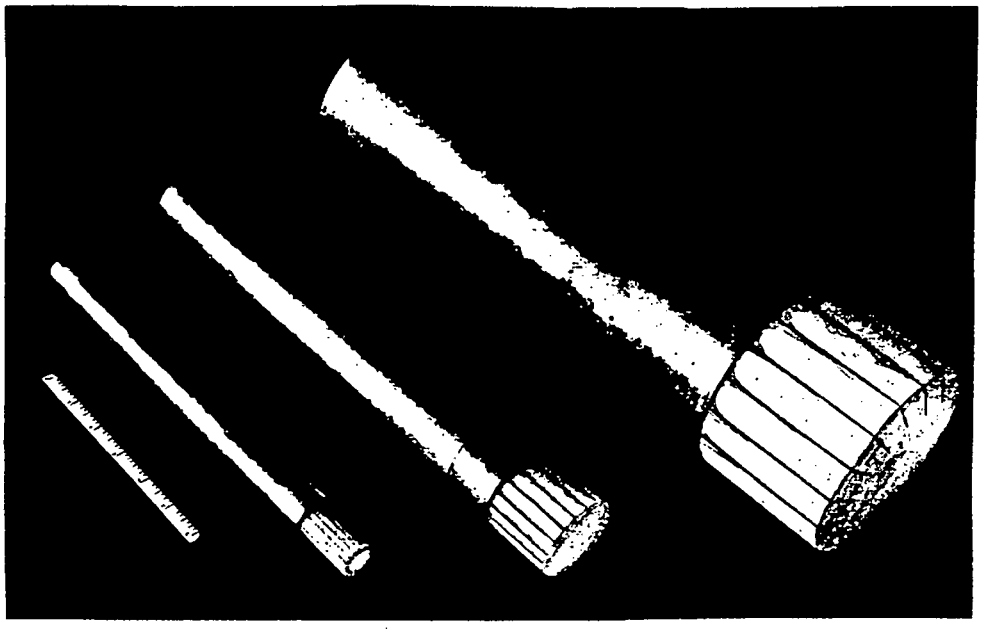

Figure 2.16. Practical TE01 circular mode filters.

These consist of a series of resistive sheets which are symmetrically arranged in a radial fashion within the guide. This forms a resistive path which is perpendicular to the electric field of the TE01 mode, which has a concentric electric field. Any other modes that have an electric field component in the radial direction, ie TM01, will be attenuated.

Actual devices which were constructed by Barlow [2.2] exhibited an insertion loss of 0.05 dB for the TE01 mode. While some of the other modes were attenuated by up to more than 20 dB.

2.6.3. Tapers.

As the TE01 mode is a high order mode it is generally launched into a waveguide of such

dimensions that it is the dominant mode, this reduces the excitation of the higher order spurious modes because of the natural filtering action of a section of waveguide as shown in Fig 2.17.

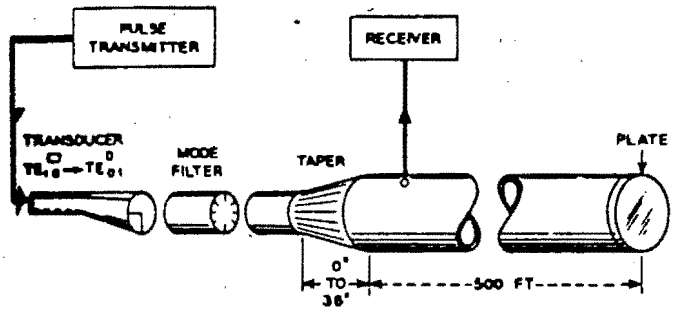

Figure 2.17. Typical taper application.

A taper section is used to connect the initial launching section to the final waveguide. This taper has to be gradual (ie relatively long in terms of wavelengths) to reduce the excitation of spurious modes. The design must also take account of the reflectional problems related to the matching of sections of waveguide. Generally the longer the taper the better its performance. Although a shorter transition can be used if a dielectric correction lens is used. Uncorrected tapers generally have to be approximately 12 to 36 wavelengths long [2.2].

2.6.4. Discussion.

This technology was extensively investigated in the fifties and sixties primarily as a telecommunications medium. Where the low loss was ideally suited for

long distance communications where the number of repeaters would be minimised by the low attenuation rate. Another benefit of using waveguide is that it offered privacy to the link as well as shielding it from interference. The bandwidth of a waveguide link was also considerably larger than any of the coaxial or other cable links that were in use at the time. Free space microwave links lacked privacy and congestion of the microwave frequency bands was occurring. The interference of climatic conditions on microwave transmissions were all reasons why attention was focussed on the use of the TE01 mode for telecommunications.

The invention of fibre optic cables has lead to the relegation of the TE01 mode to the area of pure academic interest. Although a few practical applications do however exist. The transmission of high powers from a microwave source to an antenna is one of them where the low loss and the high isolation are distinct advantages in this case.

2.7. Mode Utilisation Proposals.

2.7.1. Original concept.

The first system proposed was to use the dominant mode of a circular ore pass to propagate the radio signals. However the work of the other researchers [2.6] showed that the attenuation in the region of the theoretical cut-off frequency of the ore pass would be prohibitive. This conclusion was reinforced by the measurements taken by the author in a small tunnel. The results were shown in Table 2.1. The cutoff frequency for the fundamental mode for this

tunnel was in the region of 100 MHz. Tests at 137 MHz gave an attenuation rate of 2.70 dB/m with an estimated total attenuation of 891 dB for a distance of 330m. Thus it was shown that fundamental mode operation is not feasible due to the unacceptably high attenuation.

2.7.2. Low loss proposal.

The information presented earlier indicates that an overmoded TE01 mode would be ideal for this application as it offers low attenuation rates which would simplify the design of the unit. The literature base covering the TE01 mode is extensive and most foreseeable problems have been encountered before by other researchers. These problems had all been solved in a variety of ways, so a practical implementation seemed possible.

The proposal was to use a TE01 mode transducer at the top of the ore pass to transmit and receive the radar signal. This would have to be succeeded by a mode trap to attenuate any of the spurious modes that may be generated by the conversion process.

Any of the waveguide type transducers can not be directly implemented as the final waveguide/ore pass is 6 m diameter. The structures that would be required for efficient operation, long smooth tapers etc, would have been too large and cumbersome to deal with. Local testing of the devices would be impossible as transporting the devices to/from the mine is not practical.

2.7.2.(i) Mode transducer proposals.

These were based on the first mode transducer described in section 2.7.1., which utilises a waveguide that is split into 4 sections and feeds the circular waveguide as shown in Fig.2.13. A large steel supporting structure would have to be constructed that would be mounted over the ore pass. The feed would be a coaxial cable which is fed into a 3dB power splitter, each of the subsequent outputs is then again fed into 3 dB power splitters that yields 4 equi-power/equiphase outputs. These would then each be fed via its own coaxial waveguide transformers, to a section of waveguide which would then act as an low gain antenna. The lengths of interconnecting cable from the power splitters would have to adjusted to phase the final outputs correctly for launching TE01 and is shown in Fig 2.18.

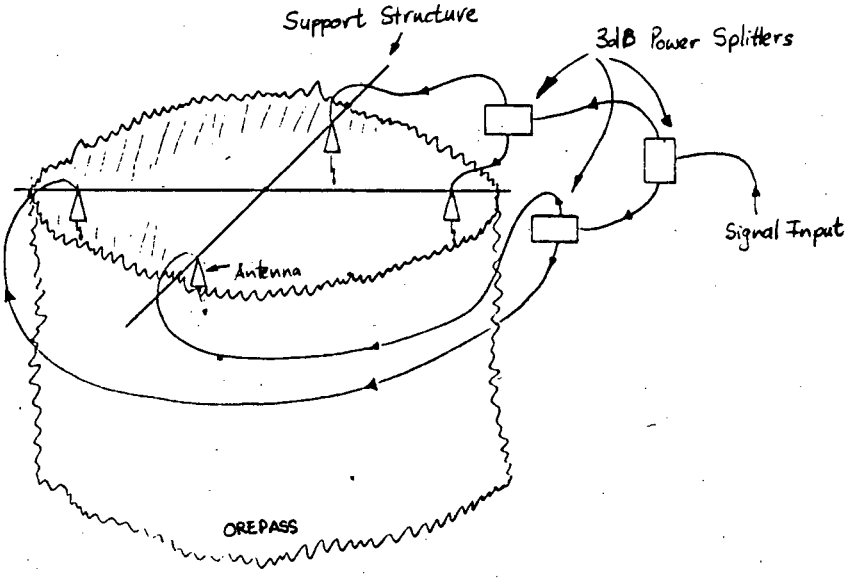

Figure 2.18. Four antenna launcher.

A simpler variation would be to omit a pair of diametrically opposite launchers, although the conversion efficiency would suffer. Adding a horn antenna to each of the waveguide launchers would enhance the performance of the transducer.

The mode trap would consist of radial steel strips attached to each other at the center, which is effectively a narrow section of one of Barlow's devices as shown in Fig 2.19.

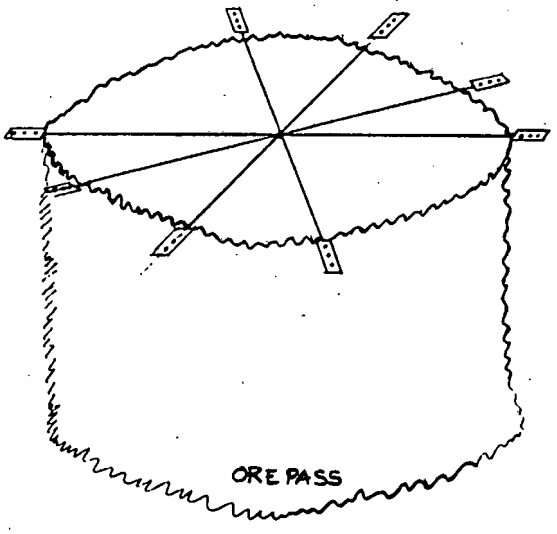

Figure 2.19. Radial mode trap.

After the first of the eight ore passes had been constructed a visit to the Finsch Mine was arranged to inspect the ore pass first hand. It was evident from the structure of the ore pass that the overmoded waveguide TE01 mode could not propagate for reasons described below. A detailed sketch of the ore pass with

the location of the level indicator is shown in Fig. 1.3.

The first 20 m of the ore pass has a diameter of 3 m afterwhich it abruptly widens to the full 6 m diameter. This is the result of the boring technique that is used to manufacture the upper section of the ore pass. As indicated in section 2.6.3., gradual tapers in cross sectional area essential for propagation in the TE01 mode, to minimize coupling into stray modes. This step discontinuity would result in a large reduction in signal power and possible collapse of the mode.

At the first tipping point on the 370 m level, 20 m down from the level indicator site, the ore pass wall is not entirely circular with a large section of it non-existent. A similar situation may arise at the other lower tipping points as these are constructed and the possibility of steel sealing doors was not considered feasible by the mine.

These gaps in the wall of the ore pass would result in a large transfer of power into other modes at each of the tipping points. Each discontinuity would require a mode trap after it to maintain the purity of the TE01 mode. But the installation of mode filters would be impractical as the ore pass still has to allow ore to feed through it.

This mode is normally difficult to implement and maintain in real waveguides but the

construction of the ore pass renders it unsuitable for this application. This information was not available at the start of the project and only became evident after visiting the Finsch diamond mine.

2.7.3. Final characterisation of the ore pass.

Fundamental mode operation is not suitable, as stated earlier, so some form of overmoding is imperative. Barlow [2.2] indicated that attenuation can be reduced by having a waveguide of large radius and consequently a small (fc/f) ratio, see equation (2.12).

Deryck [2.6] indicates that it is difficult to determine the theoretical attenuation of electromagnetic waves in a tunnel without first determining the conductivity of the wall which is in itself difficult and inaccurate. Below cut-off, where propagation does not depend on wall conductivity, the attenuation can be predicted with reasonable accuracy by equation (2.11). However the attenuation is too high for below cut-off propagation for this application. Above cut-off, the attenuation increases with the square root of the wall resistivity, and the transverse dimensions of the tunnel become more significant (2.9 & 2.10) to the resultant attenuation. The size of the tunnel is therefore of more importance than its wall conductivity as far the propagation of high frequency electromagnetic waves are concerned [2.6]. Further, the surface roughness will have a significant effect on attenuation.

Field strength tests in free space were performed using a pair of MRA7 Tellurometer electronic distance measuring (EDM'S) instruments at a frequency of 16.25 GHz using the in-built relative field strength indicator.

These tests were augmented by additional tests that involved the use of one EDM as a transmitter and a receiver consisting of an RF power meter with a range of antennae. The tests were conducted over a field with a short grass covering, in a horizontal underground tunnel (at the Finsch Mine.) and finally down the vertical ore pass at the Finsch Mine.

Table 2.2.

Field Strength Results.		
Transmit Ant.	**Receive Ant.**	**Field Str. [nW]**
Dish	Dish	1000.0
Horn	Dish	39.0
Dish	Horn	9.0
*Horn	Horn	3.5

Table 2.3.

MRA7 Tellurometer Specifications.			
Frequency	: 16.25 Ghz.	**Antenna Gains**	
Transmitter Power	: +16 dBm		
Transmitter Power	: +16 dBm	**Horn**	: +12 dBm
Distance	: 255.0 m	**Dish**	: +24 dBm

Table 2.4.

UCT Prototype Ore pass Level Monitor Specifications.		
Operating Frequency	:	10.525 GHz
Output Power	:	+16 dBm
Antenna Gain	:	+34 dB
I.F. Sensitivity	:	-115 dBm

The operational frequency was chosen as 10 GHz, ie X-Band, as sources, circulators and mixers are freely available. Scaling the above results to work over both the full range and the lower frequency is detailed below.

2.7.3.(i) Ore pass path loss calculation.

The last case, indicated with the asterisk in Table 2.2, is used to calculate the path loss, although any of the values could be used.

$$\text{Path Loss} = 10 \log (Prx/Ptx)$$
$$PL = 70.58 \text{ dB}$$

Reducing frequency results in a lower path loss,

$$\text{Path Loss Reduction} = 10 \log (f1/f2)^2$$
$$= 20 \log (10.525/16.25)$$
$$PLR = -3.78 \text{ dB}.$$

The maximum range, is required to be 350 m, therefore the path loss increase will be,

Path Loss Increase = $10 \log (d2/d1)^4$

$= 40 \log (3.5/2.55)$

PLI = 5.50 dB

Approximate losses are : PL - PLR + PLI

= 70.58 - 3.78 + 5.50

= 72.3 dB

Changing from the communication system to the radar system, ie a large transmitter dish with a passive target in place of a pair of horn antennae. The 'target' is assumed to have a radar cross-section of 0.1m x 0.1 m, dish gain taken to be 34 dB. The radar cross section of the bottom of the ore pass is unknown. It will undoubtedly vary depending on how the rocks are stacked on top of each other. However the radar cross section is not likely to be less than 0.1 m x 0.1 m.

System gain increase due to dish : 34-12 = 22 dB

Gain of target 18.2 dB ie <u>6 dB increase</u>

Approximate path loss = 72.3-22-6.2

= 44.1 dB

Due to the reciprocity of the link, this figure can be doubled for the two-way link.

Two-way path loss = 88.2 dB

Approximate mixer loss = 15 dB

Total system losses = 88.2+15 = 103.2 dB

2.7.3.(ii) Free space path loss calculation.

The path loss can be estimated by using the radar equation, see [2.19], (and equ. (2.3))

$$\text{Path Loss} = 10 \log (Prx/Ptx)$$
$$= 10 \log \frac{((G*\lambda)^2*\sigma)}{((4\pi)^3*R^4)}$$
$$= 117.2 \text{ dB}$$

Where $G = 34$ dB $= 2511.89x$
$\sigma = 0.1 \times 0.1$ m^2
$R = 350$ m

The specifications of the equipment used appears in Table 2.3. and the results appear in Table 2.2. The results indicate that the losses experienced by the signal is approximately the same as for the free space path. This indicates that the system can be designed for free space operation, with testing taking place in free space, in so doing simplifying the design/test procedure. In particular there is no requirement to do initial range measurements in a test tunnel. The propagation thus takes place without any guiding from the walls of the ore pass. The signal that impinges on the walls is scattered and does not contribute to the guiding down the ore pass. The part of the signal that does not touch the walls will reach the far end with the same power density as if it had propagated the same distance through free space with the same angle of divergence. Figure 2.20 shows this diagrammatically. The narrower the beamwidth of the launching antenna, the farther down the

first contact with the wall will occur. Final testing will have to take place over the full range down the ore pass.

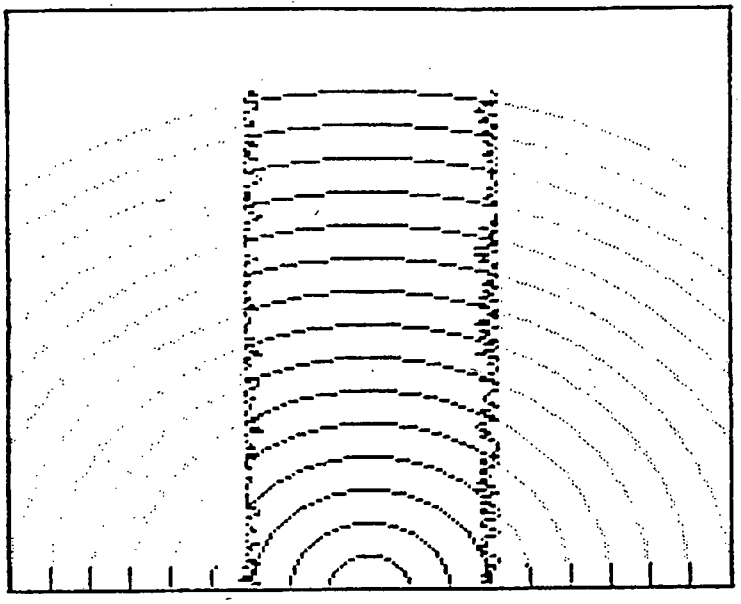

Figure 2.20. Field divergence within the tunnel.

2.8. Conclusion.

The ore pass effectively becomes a free space link if the operating frequency is high enough and the launching antenna has a narrow enough beamwidth.

2.9. References.

[2.1] AUSTIN, B.A. and LAMBERT, G.P. Electromagnetic propagation underground with special reference to mining., *Trans SAIEE*, 1985, 1-5

[2.2] BARLOW, H.E.M. and EFFEMEY H.G. Propagation Characteristics Of Low-Loss Tubular Waveguides.

[2.3] CHIBA, J. et al. Radio Communications in Tunnels. *Trans. IEEE,MTT-26*, 1978, 439-443.

[2.4] CHU, L.J. Electromagnetic Waves in Hollow pipes of Metal, *Journal Of Applied Physics*, 1938, 9, 583

[2.5] DAMOSSO, E.D. and DE PADOVA, S. Propagation and Radiation of VHF Radio Signal in Motorway Tunnels. *Trans. IEEE, VT-25*,1976, 39-45

[2.6] DERYCK, L. Natural Propagation of Electromagnetic Waves in Tunnels.*Trans. IEEE,VT-27*,(3),1978,145-151.

[2.7] EMSLIE, A., LAGACE, R. and STRONG, P. Theory of the Propagation of UHF Radio Waves in Coal Mine Tunnels. *Trans. IEEE, AP-23*, 1975, 192-205

[2.8] FRITSCH, V. Propagation of radio frequency electromagnetic fields in geological conductors, *J. Res. Nat. Bur. Std., Vol. 67D*, no.2

[2.9] GABILLARD, R. Propagation des ondes 'electromagn'etiques dans une galarie souterraine., *Revue de l'Industrie Min'erale, Vol.52*, Feb, 1970, 83-108

[2.10] GILLETTE, M.R. and GILMOUR, A.S. Attenuation Measurements in the 1 to 1000 MHz Frequency Range in Wet Granite Tunnels. *Trans. IEEE, EMC-17* ,1975 , 201-206

[2.11] IVANOV, A.A., SAKALO, L.G. and PUSKAR, M.S. Experimental determination of a frequency for radio communications., (in Russian), *Gornyi Zurnal, Vuz serie*, Vol. 13, 1968, 171-173

[2.13] KARBOWIAK, A.E. Trunk Waveguide Communication (1st ed.). Chapman and Hall, Netherlands, 1965

[2.14] LIAO, S.Y. Microwave Devices and Components (1st ed.). Prentice-Hall, Inc., 1985, 64-74

[2.15] LOVELL FOOT, J.B. Transmission Through Tunnels. , *Wireless World*, December, 1950, 456-458

[2.16] MARCUVITZ, N. Waveguide Handbook., New York, Toronto, London: McGraw-Hill, 1951, 55-72

[2.17] MILLER, S.E. and BECK, A.C. Low-Loss Waveguide Transmission. *I.R.E.*, March, 1953, 348-358

[2.18] MONK, N. and WINBIGLER, H.S. Communications with moving trains in tunnels., *IRE Trans*, VC-7, 1956, 21-28

[2.19] SKOLNIK, M. Introduction to Radar Systems (2nd ed.). McGraw-Hill, Inc. , Japan, 1980, 3-4

[2.20] TERMAN, F.E. Radio Engineering., New York and London: McGraw-Hill, 1947, 137-143

[2.21] YAMAGUCHI, Y. and SEIKIGUCHI, T. Attenuation Constants of UHF Radiowaves in Arched Tunnels.*Trans. IEEE,MTT-33*, (8), 1985, 714-718

[2.22] YAMAGUCHI, Y., ABE, T. and SEKIGUCHI, T. Experimental Study of Radio Propagation characteristics in an Underground Street and Corridors. *Trans. IEEE, EMC-28* , 1986, 148-155.

Chapter 3
BASIC PRINCIPLE OF OPERATION.

3.0. Introduction.

The previous chapter described the numerous RF and microwave tests that were undertaken to gain insight into the problem of sending radio/microwave signals down tunnels. The final conclusion was that the attenuation was approximately the same as for free-space. This means that the measurement device can be designed and calibrated for free space, with little change in performance experienced when it is installed the ore pass.

Figure 3.1. The completed prototype ore pass monitor.

The measurement system is a development of the classical frequency modulated continuous wave or FMCW radar. A radar type solution was chosen on the basis that the level of ore can act as a passive reflector to the

radar beam. The fact that ore is continually added/withdrawn from the ore pass means that an active device cannot be dropped onto the ore unless it is very cheap, which an active device will not be. There are numerous reasons for this choice of a CW implementation over say a pulse radar (AM). The mining environment is a rugged one, to which semiconductors are ideally suited. Semiconductor devices are also best operated in continuous mode, with little or no benefit derived from pulse operation. Solid state devices are readily available and cheap.

Thermionic devices, those that have some form of filament, are suited to pulsed mode systems where very high powers can be obtained for short impulse-like intervals. These devices are, however not suited to the mining environment because of the fragility of their glass envelopes and thermo-electric elements as well as the high power dissipation. Further, thermionic valve devices require power supplies of 1 kV or more which is also not suitable for the mining environment. The high power that they can achieve is suited for long distance measuring, i.e. kilometers to tens of kilometers. The range of the radar in this case is limited to less than half a kilometer. To measure range accurately over these short ranges, would involve accurate timing of the short pulses which neither inexpensive or simple.

A solid state CW radar will therefore consume considerably less power and transmit less microwave energy which are both salient features when safe underground operation is considered.

In this form of radar, the carrier is continuously active, but the carrier frequency is deviated as a function of

time, frequency modulation is applied to the carrier frequency.

3.1. Basic Principle Of Operation.

Figure 3.2. shows the installation location of the level measurement device diagrammatically where it is located on the 35 level, i.e. 350 meters below the surface.

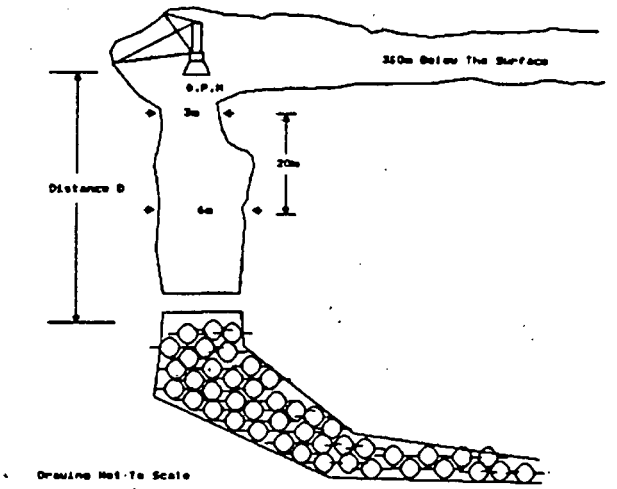

Figure 3.2. Location diagram of the ore pass monitor.

By applying elementary physics, the time t1 or signal propagation delay for a radar signal to travel from the transmitter down to the ore and back again, can be calculated.

$$\text{Propagation Delay : } t1 = \frac{2*D}{c} \qquad (3.1)$$

where D = depth [m],
c = Speed Of Light [$3.0*10^8$],
t1 = Time [s].

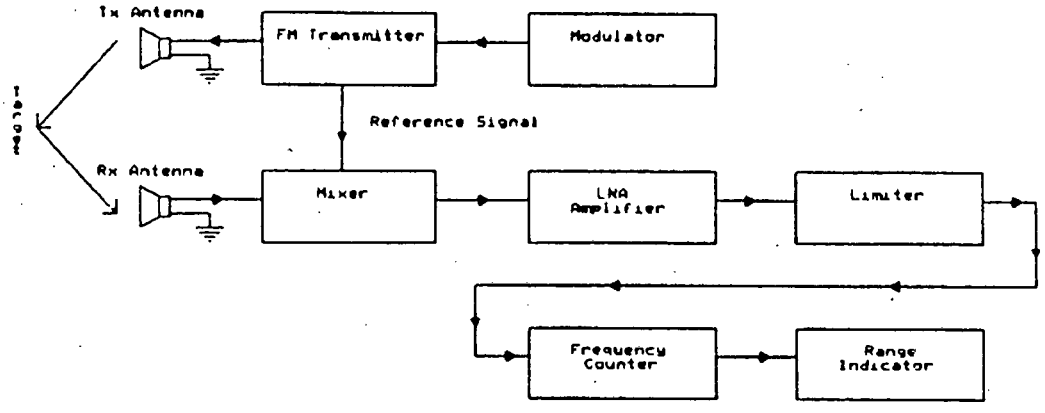

Figure 3.3. Block diagram of a FMCW radar system.

The modulator provides the modulation signal for the tunable source, if one assumes that the carrier frequency is allowed to deviate linearly, then the output of the source will be the solid line in Fig. 3.4 below. The ore located a distance D below the radar will reflect some of the incident microwave energy back towards the receiver. The time taken for this to arrive back at the receiver is t1 as calculated above in equation 3.1. This echo signal is indicated by the dashed line in Fig.3.4. If this echo signal is heterodyned with the transmitter reference signal, a beat frequency fb will be produced. If the rate of change of frequency of the carrier is fo', the beat frequency is

$$fb = fo' * t1 = \frac{2 * R * fo'}{c} \qquad (3.2)$$

where, $fo' = \delta f / \delta t.$

$$= \frac{(f1 - f0)}{(t0)}. \quad \{\text{see Fig.3.4.}\}.$$

But obviously some form of periodicity will have to be added to the modulation waveform as most practical tunable sources have a limited linear tuning range and/or a maximum allowable deviation, a triangular modulation waveform was chosen as it consists of a linear increasing and a linear decreasing time-ramp. But the waveform does not necessarily have to be triangular, it can be sinusoidal, sawtooth or any other shape. The beat frequency for triangular modulation is shown in Fig. 3.5., it's frequency is constant except at the turn-around region, when it ramps down to zero and then up again. If the frequency is modulated at a rate fmod over a deviation of δf, the beat frequency will be

where $1 / t0 = 2 * fmod$ {from Fig. 3.4.} (3.3)

and hence $fo' = \delta f * 2 * fmod$

therefore $$fb = \frac{2 * R * 2 * \delta f * fmod}{c}. \quad (3.4)$$

Thus by measuring the frequency of the beat frequency the distance D can be inferred. [3.1].

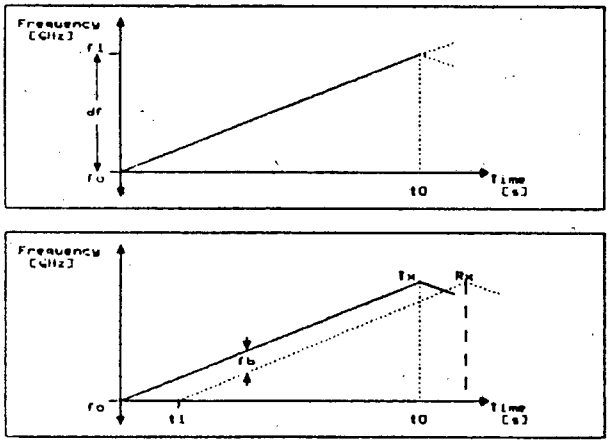

Figure 3.4. Transmitted and time delayed received radar signals.

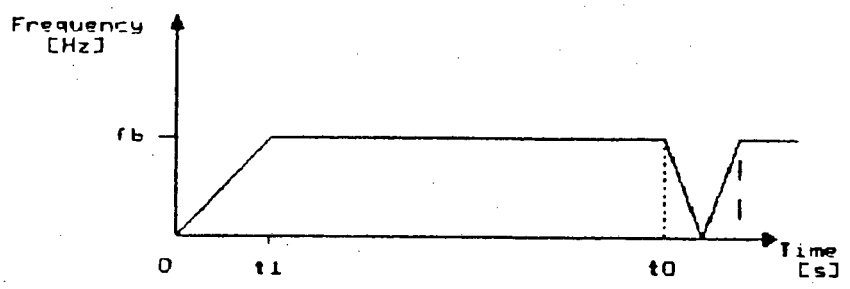

Figure 3.5. Frequency difference between transmitted and received signals.

3.2. Basic Hardware Description.

The modulator produces a periodic triangular waveform that forms the basis of an FMCW radar as it controls the frequency variations of the transmitter.

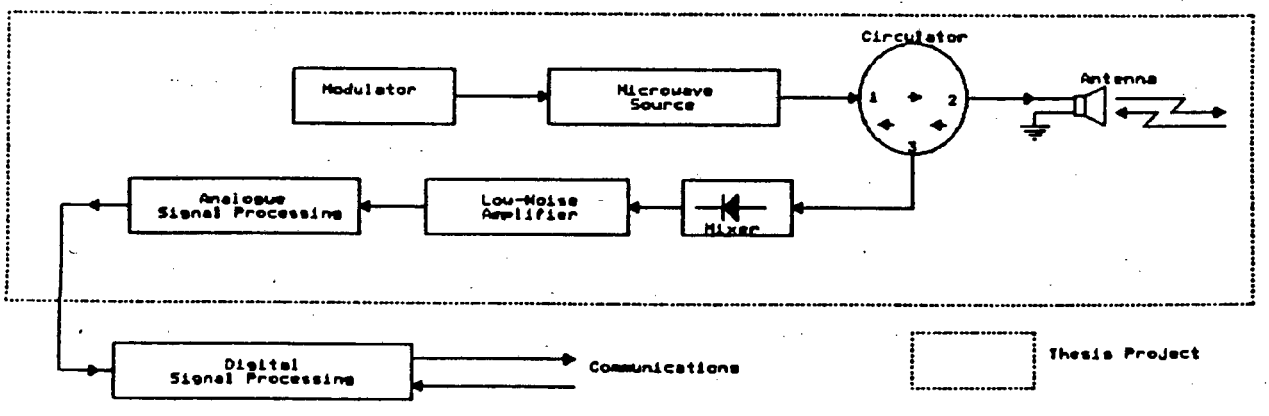

Figure 3.6. Block diagram of the ore pass monitor.

It determines the center operating frequency of the microwaves and the maximum frequency deviation that can occur.

Ideally the waveform should be exactly triangular, i.e. linear-time ramps of increasing and decreasing magnitude but in practise non linear waveforms have to be used. In an attempt to linearise or minimise the non-linearities of the tunable source.

The CW source or the transmitter is a solid-state oscillator that is able to have it's frequency electronically tuned.

The combination of the modulator and the source constitute the FMCW transmitter, where the modulator output is applied to the frequency control input so that the microwave frequency will vary in unison with the modulator output voltage.

The microwave output is then coupled to the circulator which is a 3 port microwave device, which allows a single antenna to be used in place of the two in Figure 3.3. but still allows the transmit and receive signals to be separated.

The circulator only allows signals to pass in the directions indicated by the arrows, ie from port 1 to port 2, port 2 to port 3 and from port 3 back to port 1.

The source is located at port 1, the antenna at port 2 and the mixer is located at port 3. Therefore the microwave output (port 1) will pass from the source to the antenna (port 2), where it will be launched into the ore pass. Reflected signals will impinging on the antenna will be passed on to the mixer (port 3). The mixer is well matched and does not allow signals to pass back to port1. However, the antenna's match is also not exact so that a small amount

of the source's output will be included with the signals from port 2 to port 3. The mixer will therefore have two signals incident on it, the reflected signals from the ore and a reference signal from the local oscillator.

The mixer diode is a device that heterodynes incident signals because of its nonlinear transfer characteristic, providing that there is a large amplitude difference between the input signals. The heterodyning process generates numerous frequency components, but this application is only concerned with the difference frequency components of the two input signals. The beat signal therefore is obtained by filtering the output of the mixer.

The mixer output is minute as the antenna only receives a small amount of power and it requires a large amount of gain before it can processed in any way. The low-noise amplifier amplifies the difference frequency component without degrading signal to noise ratio. The output of the low noise amplifier has a main frequency component that is dependant on the distance between the radar unit and the level of ore, the 'target' in this case. It will also contain other frequency components that correspond to side wall reflections and any other discontinuities in the ore pass.

The inherent bandwidth limitation of the amplifier filters signals but more exact filtering is required and this is achieved by the post-amplification or signal processing filters that have accurately defined cut-off frequencies. These filters serve to minimize the effects of close-in signals as well as multipath signals. They also limit the frequency of the return signal to those that correspond to the completely empty and completely full conditions of the ore pass.

The filtered signal then undergoes processing in the signal processing block, which analyses it and then calculates the depth of ore in the ore pass.

The signal processing block can be any device that can do frequency analysis, however in the final version, it should be a signal processing computer as the level of ore has to be communicated to the surface control computers, as well as an indication of any error condition within the unit. However for testing purposes and for system validation, this investigation was restricted to the use of a spectrum analyser for the frequency analysis.

3.3. Reference.

[3.1] SKOLNIK, M. Introduction to Radar Systems (2nd ed.). McGraw-Hill Inc., Japan, 1980.

Chapter 4
DESIGN OF INDIVIDUAL MODULES.

4.0. Introduction.

This chapter is concerned with the design of the circuitry that constitutes the ore pass level indicator. The specifications for the various modules together with the design constraints as well as the reasons for the various circuit configurations are also described.

The modules are described in the same order as they were mentioned in the previous chapter.

4.1. The Modulator.

4.1.1. Circuit description.

This circuit block provides the modulation signal, which ideally should be triangular, but may have to be distorted in order to correct for non-linearities in the subsequent modules of the system.

The microwave source's operating frequency is dependant on the DC bias voltage applied to the varactor, see later, therefore the modulator must be able to provide both an adjustable DC offset and an adjustable amplitude signal. These set the lowest microwave output frequency, the start frequency of the sweep, and the maximum deviation from the start frequency respectively.

The frequency of the modulation waveform must also be adjustable in order that the frequency of the IF

signals can be constrained to a restricted band of frequencies.

It consists of 4 subsections, a variable frequency oscillator, an up/down address counter, a transfer map and a digital to analogue conversion and level shifting stage, as is shown in figure 4.1(a).

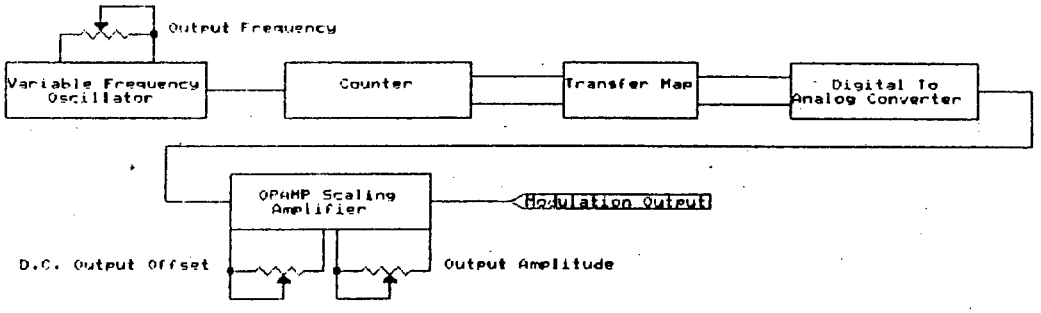

Figure 4.1(a) Block diagram of the modulator.

Most of the circuitry is digital and was specifically designed that all of the above mentioned parameters can be independently adjusted.

Table 4.1.

Specifications of the modulator.	
Maximum modulation frequency	391 Hz
Minimum modulation frequency	3.5 Hz
Maximum output voltage	+10.8 Volts
Minimum Output voltage	-10.8 Volts
Maximum amplitude of modulation waveform	+5.0 Volts
Minimum amplitude of modulation waveform	220 mV.

4.1.2. Circuit details.

The variable frequency oscillator is based on the voltage controlled oscillator subsection of the micropower CMOS phase locked loop integrated circuit, the 4046, which was chosen as it offered ease of use, only two external components to configure the oscillator, as well as low power consumption. It also offers good long-term stability of it's operating frequency and is easily re-tuned.

A CMOS device was chosen over an equivalent TTL device as the CMOS device offered a much lower power consumption.

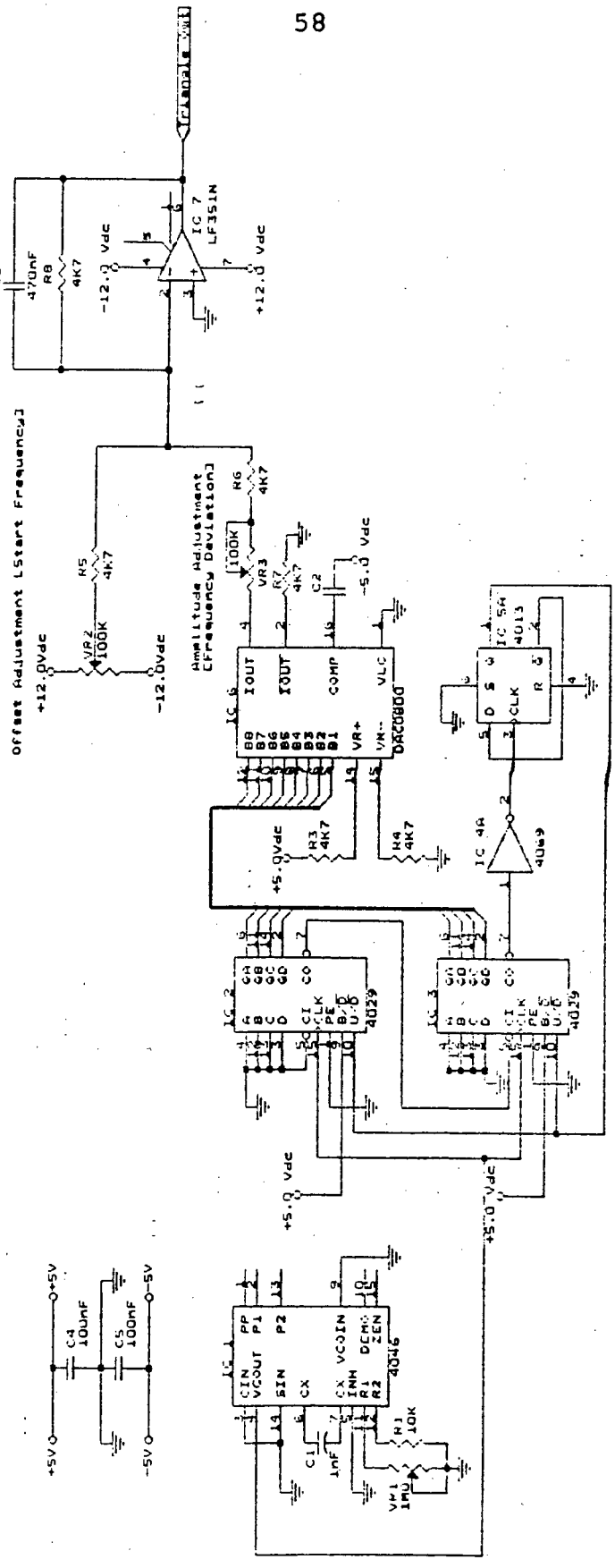

Figure 4.1(b) Complete schematic of the modulator.

Figure 4.1(b) shows the complete circuit diagram of the modulator. Resistor, R1, and capacitor, C1, are the main frequency determining components of IC1, the oscillator. These two components together with VR1, form the complete frequency determining network. Variable resistor, VR1, allows the output frequency on pin 4 of IC1 to be adjusted. The range of frequencies available is from 1786 Hz to 200 kHz. This is considerably higher than the maximum modulation frequency quoted in table 4.1. The reason for this is that the up/down counter is used to generate the triangular waveform, see later, subsequently the input frequency, to the dividers, needs to be higher than the required output frequency.

The temperature coefficient and the long-term stability of the oscillator is essentially dependant on the respective coefficients of the passive components C1 and R1. As IC1 has a temperature coefficient of 0.12 %/°C when operated on a 5V supply. The counter consists of two 4 bit programmable up/down counter chips, IC2 and IC3, which are CMOS 4029 devices. They can be programmed to count up or down, in binary or in binary coded decimal (BCD) depending on the inputs applied to the chips.

The up/down counter is 8 bits wide, a count-up sequence will take 2^8 input clock cycles. Similarly a count-down sequence will take 2^8 clock cycles. Hence a complete count up/down cycle will take $2*2^8$ or 512 clock cycles. Formally a complete up/down cycle will take $2^{(b+1)}$ clock cycles to complete.

Each chip has a carry-out pin which is used to cascade the devices together to expand the total number of bits in the counter. This signal is in the form of a

short pulse that is used to increment the succeeding counter.

The counters are configured for full binary counting mode with the carry-out of the least significant nibble (LSN) counter connected to the carry-in pin of the most significant nibble (MSN) counter. The carry-out pin of the MSN counter is inverted, logically, by IC4(a), a 4069 chip that contains six inverters. This signal drives the clock input of a D-type flip flop, IC5(a), that is configured as a toggle flip flop. A toggle flip flop's output is the clock input divided by two. IC5, a 4013, contains two D-type flip flops. The output of the toggle flip flop drives the U/D pins of the counters thereby determining the direction in which they count.

Counter operation will be as follows :

Assuming that the counters are reset, all outputs at logic '0' (pins 6,11,14,2 on IC2 and IC3),on power up. As each clock pulse arrives the two counter chips will count-up, progressing through all of the 256 possible permutations of states on the 8 outputs.

As the last state is reached, all outputs at logic '1', the carry-out signal of the MSN counter will pulse high. The inverted pulse (IC4(a)) will trigger the toggle flip flop (IC5(a)), toggling it's output which will change the count direction lines of the counters, forcing the count-down sequence to be initiated. When the all zero state is reached, the carry-out will again pulse which will force a direction change and the sequence will be repeated as long as the clock pulses are provided.

The count-up and count-down sequence take the same time, 256 input clock pulses, therefore the output signal has a 50% duty cycle. Figure 4.2 below shows the same count sequence for a single 4 bit counter.

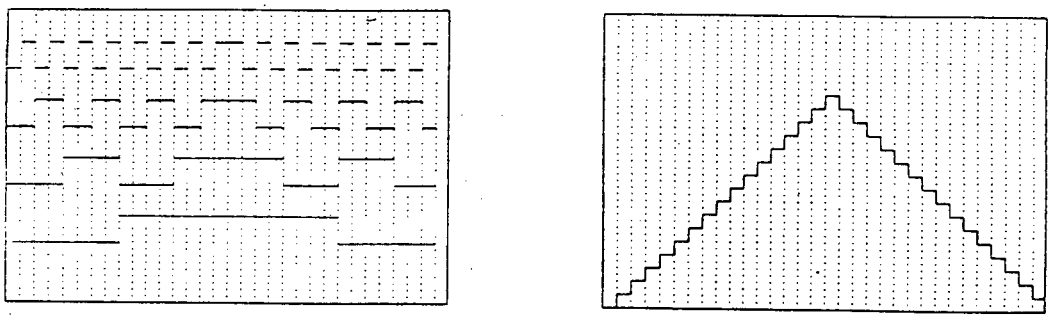

Figure 4.2. A 4 bit count-up/down count sequence and analogue conversion.

The transfer map in figure 4.1(b) consists of a straight-through wired connection. However the circuitry has been designed in such a way that this can be replaced by an EPROM, an erasable programmable read only memory, device. Which will be used to correct or linearise the distorted tuning characteristic of the varactor in the microwave source.

The 8 output bits of the counter are to be connected to the 8 least significant address lines, the other unused address lines tied low, so that the counter will address the EPROM's first 256 locations, first in increasing order then in decreasing order, ad infinitum.

As each location's address appears on the address lines, the EPROM will output the data byte stored at

that location on the 8 bit data bus. The digital to analogue converter would be connected to this bus, it would then convert the digital word into it's equivalent analogue voltage. The counter together with the EPROM would be the hardware equivalent of the look-up table that is commonly used in software.

The wired through connection of figure 4.1(b) has the effect of sending out a linear time-ramp first up, then down as the count sequence progresses. Figure 4.2 also shows this on a smaller scale for 4 bits.

The digital to analogue converter (DAC) and level shifting stage consists of the remaining two chips, IC6 and IC7. These are the DAC 0800 digital to analogue converter and a bifet operational amplifier (opamp), the LF151. Also referred to as the D to A stage.

The DAC converts the 8 bit digital word applied on its 8 bit data bus to a scaled analogue current using the following formula :

$$Iout = Iref * \frac{Ninput}{256}$$

This current output is applied as one of the inputs to a virtual earth inverting summing amplifier. The other input of the summer is an adjustable DC input.

The summer has unity gain inversion for both its inputs, however the DAC output amplitude is adjustable. The gain for the two inputs can be calculated using the inverting opamp amplifier configuration as follows:

$$Vout = - Vin * \frac{Rf}{Ri} \qquad \text{or Gain} = - \frac{Vout}{Vin} = - \frac{Rf}{Ri}$$

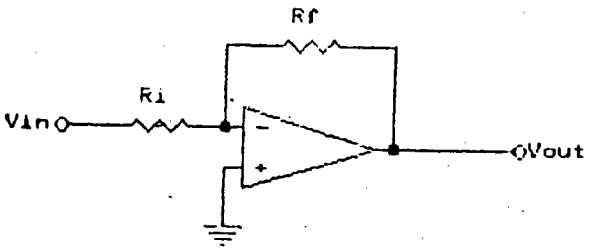

Figure 4.3 Inverting OPAMP amplifier configuration.

The adjustable DC input has, therefore, a gain of -(4k7/4k7) = -1. For the DAC output the gain is from -1 to 0.0449.

Resistor, R7, connected to Iout of the DAC is the load for the second output of the DAC, it provides two bipolar outputs. This output although not used in this case must be terminated in a load.

Capacitor, C2, is a compensation capacitor that is required for the DAC 0800 to have a stable output as it changes states, with no ringing or oscillations.

Capacitor, C3, which is connected across the feedback resistor of IC7 has two purposes, firstly to limit the bandwidth of the stage which filters the step-wise output of the DAC to produce a smooth triangular output waveform.

It also reduces the possibility of the opamp oscillating and improves the stability of the stage.

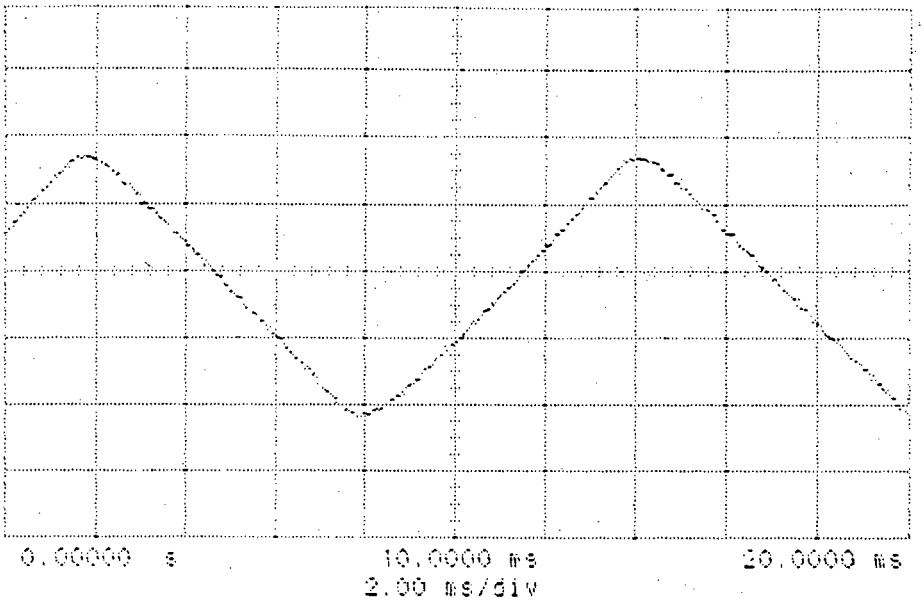

Figure 4.4. Filtered output of modulator.

Variable resistor, VR2, adjusts the DC offset, and VR3 adjusts the peak to peak amplitude of the triangular waveform, riding on the DC offset, by adjusting the gain for the triangle input.

By applying the counter output directly to the D to A stage, a variable frequency symmetrical triangular waveform can be obtained. However if the EPROM map is used any arbitrary waveform can be generated. An improved modulator circuit diagram appears in appendix-a.

4.2. The Microwave Power Source.

The source is an integral part of the transmitter/receiver device that is manufactured by Microwave Associates, inc. The device is called a 'Gunnplexor™' and has application in

many fields. Burglar alarms, voice communication links and doppler speed indicating devices are only a few examples.

Table 4.2.

Gunnplexor Specifications @ Ta = 25 °C.	
RF Center Frequency	10.525 GHz
Tuning Mechanical Electronic Linearity Frequency Stability	 ± 50 MHz 55 MHz 1 to 40 % -350 kHz/°C. max.
RF Power vs. Temperature and Tuning Voltage	 6 dB max.
Frequency Pushing	15 MHz/V max.
Input Requirements Input Voltage Maximum Operating Current Tuning Voltage	 +10.00 VDC 500 mA. +1 to +20 VDC
Noise Figure	< 12 dB
RF Output Power	40 mW min.

It consists of essentially three modules, namely the Gunn oscillator, a circulator and a mixer stage.

The Gunn diode oscillator is the heart of the system which generates the microwave power.

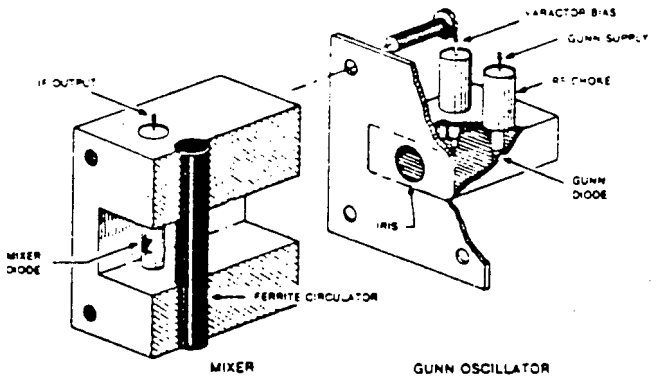

Figure 4.5. Assembly drawing of Gunnplexor™ module.

The Gunn diode is mounted together with a varactor diode in a small resonant cavity. When a regulated DC bias is applied to the Gunn diode, it oscillates. The frequency of this oscillation is determined by the dimensions of the cavity, the capacitance of the varactor diode and the two mechanical tuning screws mounted in the cavity. These screws are essentially coarse tuning controls and are factory-set for the appropriate frequency range. The capacitance of the varactor diode is determined by the DC bias applied to it. The higher the voltage, the lower the capacitance and hence the higher the output frequency. Hence this voltage tunes the output frequency electronically through a minimum of 55 MHz. The voltage tuning range of the varactor is from +1 to +20 Volts DC with the corresponding frequencies of 10.495 GHz and 10.550 GHz. Figure 4.6 shows the complete tuning characteristic of the Gunn source. The maximum output voltage available from the modulator however is only 10.8 Volts.

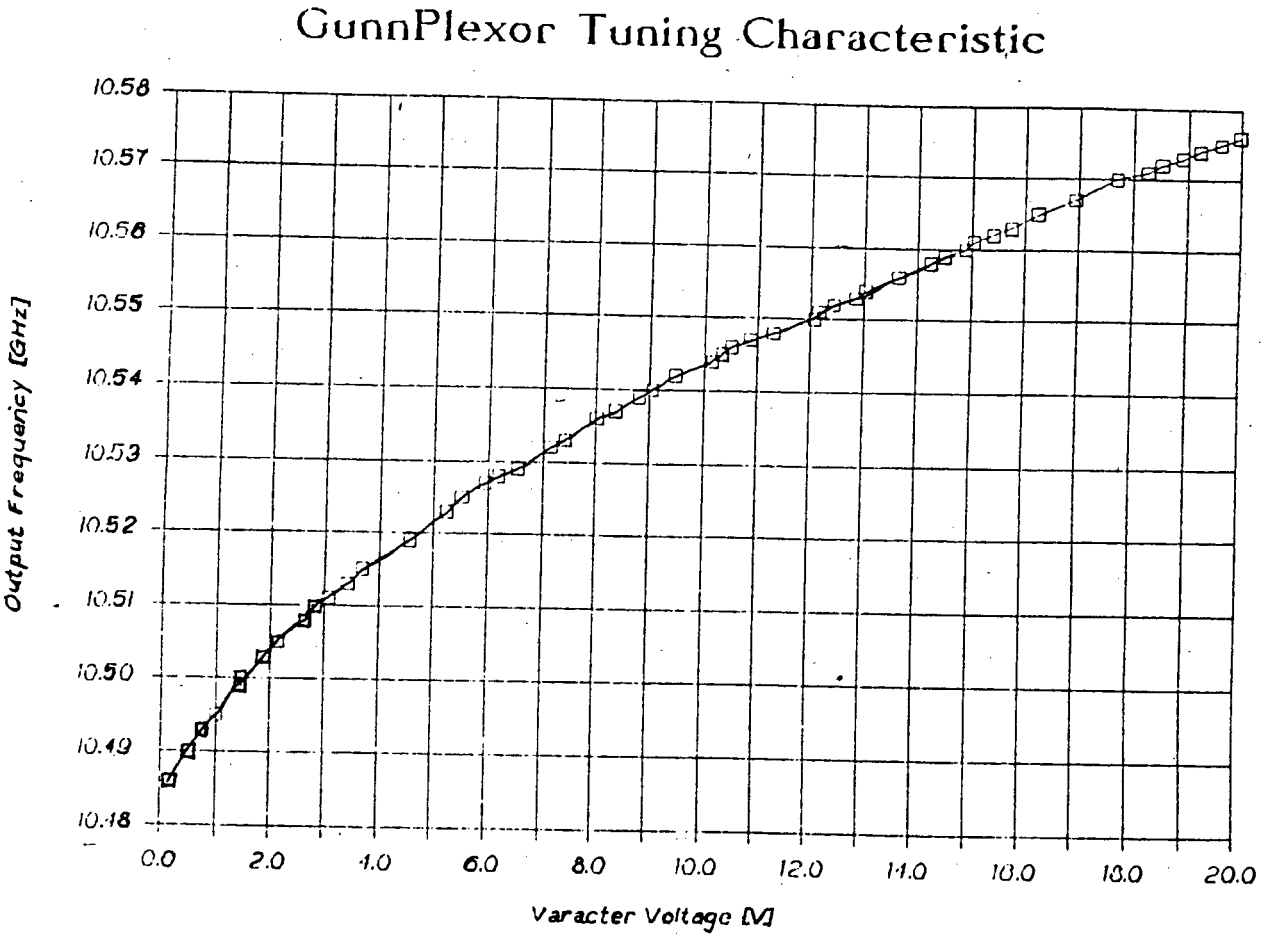

Figure 4.6. Tuning characteristic of Gunnplexor™ module.

Microwave power is coupled out of the cavity through a small iris that has been designed as a compromise between maximum power output and isolation from variations in mixer diode and load impedance. The microwave output is available on a UG-39/U standard X-band waveguide flange which is integral to the circulator/mixer housing.

The Gunn oscillator is also used to provide the local oscillator signal for the mixer diode. The ferrite circulator couples the correct amount of power into the low noise mixer diode as well as isolating the transmitter and receiver components. It also directs any incoming microwave signals to the mixer diode.

The IF output at the output of the mixer, is available at the output of an inductor/capacitor (LC) filter network that

is connected to output of the mixer diode. See Figure 4.7. The inductor, L, provides a DC path return for the mixer diode that enables it to set up a DC current through the inductor by the rectification process. The correct DC current must be flowing through the device if optimum performance is to be achieved.

4.2.1. Mixer Theory.

Figure 4.7 shows the commonly used symbol that is used to denote a mixer. A mixer usually has two signal ports, namely the local oscillator input (LO input) and the signal input port (RF input). It has one output port, called the intermediate frequency output (IF output). The two inputs, in this case appear on either side of the mixer cavity with the LO signal coming in from the Gunn oscillator while the RF signal entering directly opposite this. The IF output appears as the current that flows through the mixer diode.

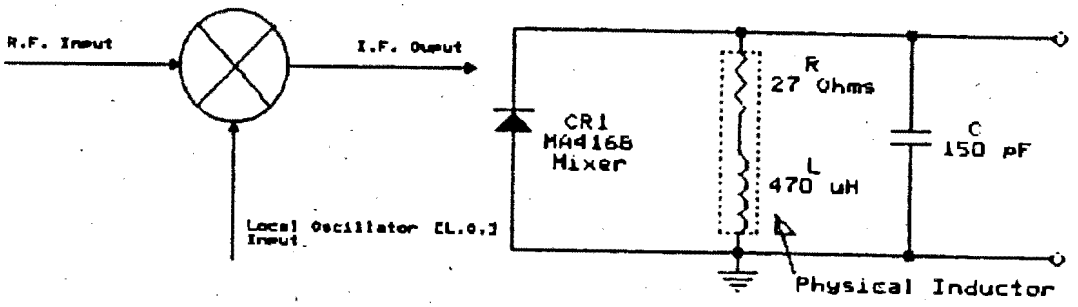

Figure 4.7. Mixer schematic.

The local oscillator input is usually very much larger, in amplitude, than the RF signal, in the order of 20 dB or more. Due to the large amplitude of the LO signal, the mixer diode can be modelled as Figure 4.8 (b). Where the diode is effectively a switch that is activated by the LO signal. The large signal flips the

diode from the forward biassed condition to the reverse biassed condition alternately. Due to the small size of the RF signal it is unable to affect this switching action.

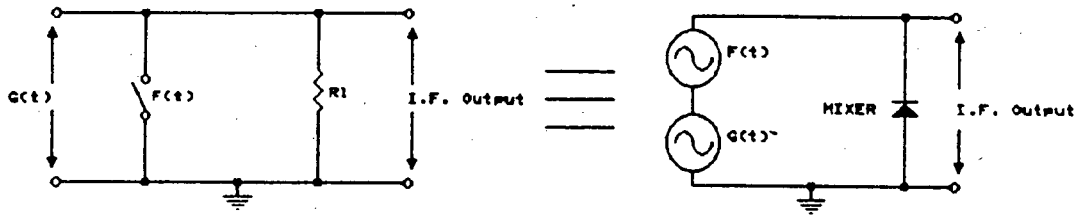

Figure 4.8. Mixer model.

The LO signal can be modelled as F(t) in Figure 4.9., having a value of either 0 or 1 because of the switching and the clamping effects of the diode. Using a general input signal, G(t), will give rise to the output signal of Figure 4.10. Where there is only an output when the LO signal has unity magnitude. The scale between the two signals has been greatly exaggerated.

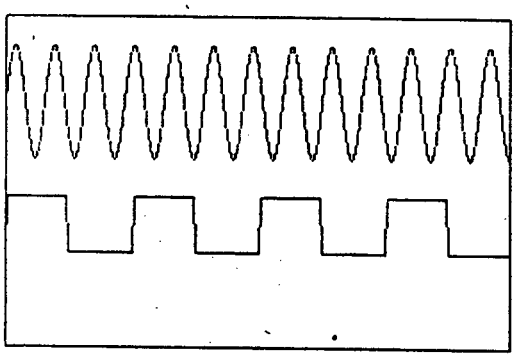

Figure 4.9. Mathematical input signals.

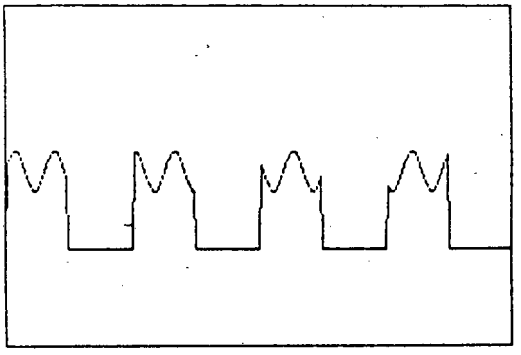

Figure 4.10. Mathematical output signal.

Analytically the LO signal, the squarewave, can be represented by the Fourier series below.

$$F(t) = \frac{1}{2} + \frac{2}{\pi} * \cos(wl*t) - \frac{2}{3 * \pi} * \cos(3*wl*t) + \ldots$$

When this waveform is multiplied with the RF signal, $G(t) = \cos(ws*t)$, the output will be :

$$O(t) = F(t) * G(t)$$
$$= \frac{1}{2} * \cos(ws*t) + \frac{2}{\pi} * \cos(ws*t)*\cos(wl*t) - \frac{2}{3 * \pi} * \cos(ws*t)*\cos(3*wl*t) + \ldots$$

(Note that amplitudes for both signals has been assumed to be unity.)

The first term is RF breakthrough or leakage into the IF output. The second term can be expressed as the sum and difference of its two component frequencies using the trigonometric identity below. By expressing the

signal in this form, the wanted signal, the second term in the O(t) below, becomes evident.

$$\cos(a) * \cos(b) = \cos(a+b) + \cos(a-b)$$

$$O(t) = \frac{1}{\pi} * \cos\{(wl+ws)*t\} + \frac{1}{\pi} * \cos\{(wl-ws)*t\} + \ldots$$

The two signals F(t) and G(t) are microwave signals and the frequency difference between them is very small, the order of kilohertz. By attenuating signals above 10 kHz all RF signals can be excluded and the difference component or beat frequency is obtained.

The mixer has to be well matched, at microwave frequencies, to minimize the reflection of any received signals back out of the RF port.

The output LC filter, Fig.4.7., attached to the IF output also forms a low-pass filter that reduces the breakthrough of any microwave signals, by only allowing low frequency signals to pass. By limiting the bandwidth, it reduces the total amount of internal noise that the system generates thereby improving the performance of the whole system. The inductor has a DC series resistance of 27 Ohms (Ω), which provides the optimum DC load for the mixer diode, where it produces the best signal to noise ratio performance.

The Gunnplexor™ module was chosen as it offered a moderately cheap, high performance alternative to using individually designed and constructed modules. Individual modules would however have had a performance advantage but a distinct cost and size disadvantage. Problems with delivery delays of

individual elements were circumvented by using the Gunnplexor™.

4.2.2. Determination of Output Impedance of IF Filter/Mixer Network.

The Gunnplexor™ module's Gunn diode was connected to a power supply of +10.0 V DC, +5.50 V DC was connected to its varactor, this allowed oscillation at 10.525 GHz.

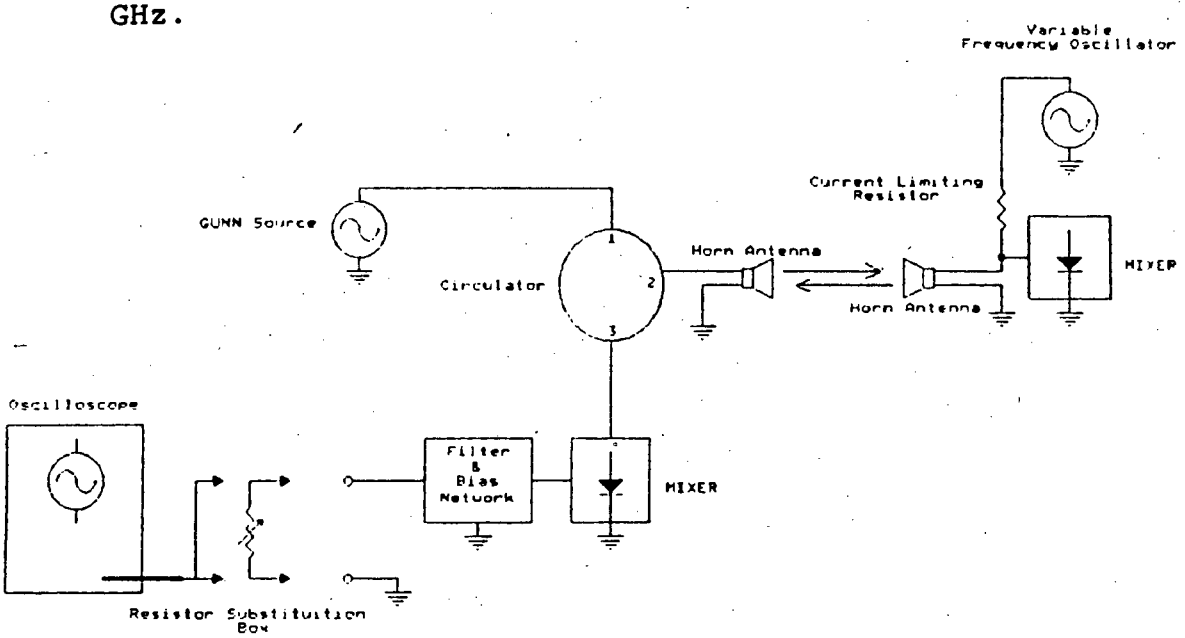

Figure 4.11. Equipment configuration used to determine the IF output impedance.

A small X-band horn antenna was attached to the waveguide flange, to enable the transmission and reception of signals.

A separate mixer cavity with its own X-band horn antenna was placed a short distance away from the first module. A modulating signal, with a variable frequency and a constant amplitude of +1.0 Volt peak to peak, was applied to this mixer diode via a current limiting resistor.

When the Gunn is activated, it transmits a microwave signal that is directed by the antenna. When the two antennae are aligned, the second antenna, will reflect any incident signals back along the same path. However there is a diode at the rear of the antenna that is being switched into and out-of conduction. This has the effect of placing a short at two different locations depending whether the diode is forward or reverse biassed. When the diode is not conducting, it has a high impedance and the rear wall of the mixer cavity will terminate the waveguide. However when the diode is conducting then it will act as a short circuit thus terminating the waveguide. When the diode is conducting it will also absorb a small amount of the incident microwave signal. Hence the reflected signal will have a small amount of amplitude modulation and a small amount of phase modulation applied to it. Because of the difference between the transmitted signal and the received signal, an IF output will be observed on the output of the LC filter.

By loading the output with a resistor substitution box and changing the effective load resistance while observing the peak output voltage on an oscilloscope, one can determine the source impedance of the network. The resistance is lowered until the peak output voltage drops to 50% of the initial unloaded output voltage. Then the output impedance of the network is indicated by the value indicated on the resistor substitution box.

The impedance was measured at three discrete frequencies in over the system's bandwidth, 100, 1000 and at 10 000 Hz. The respective impedances were 200,

230 and 210 Ohms. A effective output impedance of 220 Ohms was assumed for the whole band.

4.3. The Antenna.

Figure 3.1 showed the completed prototype ore pass level indicator. The choice of antenna is governed by design constraints as with any other part of the system. The principle design characteristics for the required antenna are quoted from Clarricoats.[4.1].

These are :

i) A relatively narrow beamwidth radiation pattern that remains relatively independent of frequency over the swept band, this also corresponds to a high gain. The high gain is required to achieve the range performance as the calculations in chapter 2 show. Similarly the narrow beamwidth is required to reduce the divergence of the radar signal and side wall contact.

ii) A relatively low input VSWR which should essentially be frequency independent over the swept band. This is to minimise the reflection of power at the transmitter which would be a loss of valuable transmitter power.

iii) It should exhibit low side-lobes as these would make alignment of the system difficult, the operator would find it difficult to determine what lobe he is beamed up on. Transmitter power would also be wasted by illuminating the side walls near the top of the ore pass.

iv) It should have a compact rugged construction because of the environment where the system will be utilised.

The antenna, shown in Fig.3.1. used on the prototype is a prime focus dipole fed parabolic dish. It has a diameter of 25 cm, and an approximate gain of 26 dB. In Chapter 2 the range calculations showed that an antenna of approximately 34 dB. gain would be required to be able to operate over the required range. This antenna has a diameter of 60 cm and is a prime focus horn fed parabolic dish. The dish was imported from England where they are used for TV satellite reception. The feed however was locally constructed especially for this application. The drawimgs for this antenna appear in appendix-c.

4.4. The Low Noise Amplifier.

4.4.1. Circuit description.

The low noise amplifier (LNA) must amplify the weak signal that is obtained from the mixer output filter without degrading the signal to noise ratio, so that signal processing of the signal can take place to ascertain the amount of ore in the ore pass. It also contains the necessary filters that have to be included to remove unwanted signals from the IF output. The IF output contains numerous spurious signals from close-in projections etc.

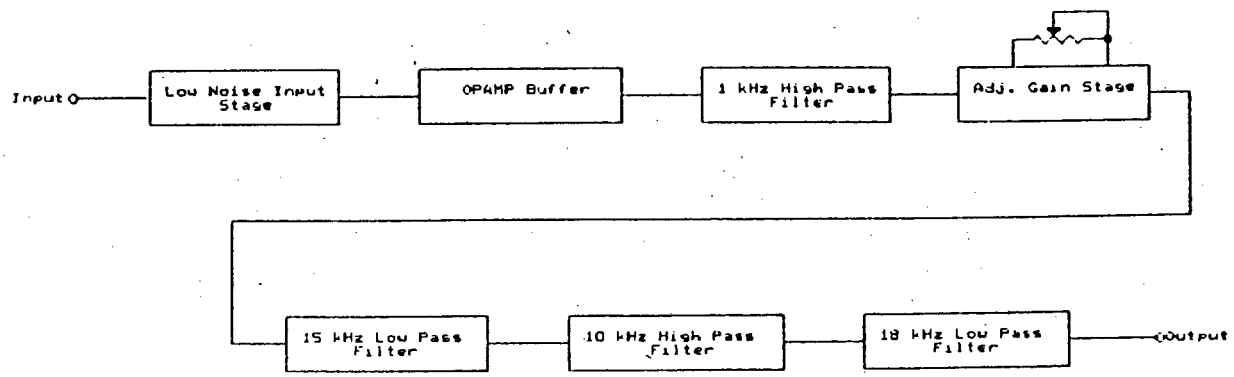

Figure 4.12. Block diagram of the low noise amplifier.

It consists of a cascaded number of amplifying stages and filtering stages. Numerous integrated circuit amplifiers were tried as the front end, but generally were found to limit the sensitivity of the receiver. The input stage, which provides the majority of the gain, is a discrete design. A transistor input stage was chosen with an input impedance of similar magnitude to that of the mixer diode. Therefore the input stage was closely matched to output impedance of the mixer filter thereby maximising the signal to noise ratio.

The output of this stage is buffered by an opamp configured as a non-inverting unity gain amplifier, which prevents the following stages from loading the output of the input stage.

The buffer is followed by a series of cascaded filter stages of the Sallen and Key type. The first is a 1 kHz high pass filter with a quality factor (Q) of 0.7. A filter with a low Q such as this does not exhibit any peaks in its frequency response. Any peak could be misinterpreted as a false level of ore. The 1 kHz filter defines the lowest frequency that can pass through the amplifier chain. It therefore determines the shortest range that the radar will ultimately be able to measure. Another use, is that it prevents the breakthrough of the modulation signal onto the output. This leakage is due to the a small power variation in the Gunn oscillator's output power as it is swept, finds its way out of the mixer.

A variable gain stage follows, it's function is to boost the signal before the final filters The gain is variable in order that the system can accommodate the variety of conditions that were found when testing the

unit with different antennae and at different locations.

Two more low pass filters succeed the gain stage, with a cut-off frequency of 15 kHz and 18 kHz respectively. Their purpose is two-fold as they limit the noise bandwidth, which improves the signal to noise ratio. They also limit the maximum frequency, thereby defining the maximum measurable range, as well as acting as anti-aliasing filters for any digital signal processor that is to be added.

Finally there is a high pass filter with a cut off frequency of 10 kHz. Its purpose is that of a range compensation filter. As was mentioned in Chapter 2, the signal strength from a target decreases at a rate of 12 dB for a doubling of distance. But as doubling the distance results in a doubling of the time delay between the transmitted signal and the received signal, it also results in a doubling of the IF beat frequency output. Therefore as range doubles, the target signal strength falls by 12 dB, similarly its frequency doubles (increases by an octave), therefore effective slope of the signal strength is 12 dB/octave.

The last filter is a second order (12 dB/Octave roll-off rate) with a cut off frequency of 10 kHz. It compensates for the loss of signal strength as the range increases by increasing the effective gain of the amplifier (at a specific frequency and hence range). The effect of this is that a constant signal to noise ratio should be maintained over the whole of the measurement range of the instrument.

Table 4.3.

Low noise amplifier specifications	
Bandwidth	9 kHz
Noise floor	-120 dBm
Total Power Consumption	0.5 W
Supply voltages	±12 & ±5 V.

4.4.2. Circuit details.

The full circuit schematic diagram of the receiver appears in Figure 4.13. Transistor, TR1, a BC109C, is a low noise, high current gain audio transistor that is optimised for audio signals. Hence it is ideally suited to this application where the IF signal frequency is restricted to 10 kHz.

Resistor, R4, and capacitor, C6, form a low pass filter network on the DC supply to the front end. This filter reduces any power supply residual noise and effectively decouples the front end supply from all the other modules supplies.

Capacitor, C2, a 1uF non-polarised capacitor is the DC blocking input capacitor. It prevents the DC voltage developed by the mixer from entering the amplifier chain where it would upset the quiescent DC conditions of the amplifier. Its also couples in the AC signals from the mixer to the base of the transistor. The lowest frequency signal that can pass from the mixer to the LNA is 723 Hz.

This can be determined by the following formula :

$$f_{(-3dB)} = \frac{1}{2.\pi.R.C}$$

where in this case R is 220 Ohms
and C is 1.0 uF

Resistors, R1 and R3, are connected as a potential divider, which takes the +12.0 V DC and produces a lower voltage to bias the transistor. The voltage at the base of transistor, TR1, is,

$$+12.0 * \frac{(3300)}{(3300+15000)} = +2.16 \text{ Volts.}$$

Capacitor, C3, decouples the potential divider to ground, thereby lowering the bias chain impedance as well as shunting any power supply noise to ground. It also reduces thermal noise generated in the biassing network.

Resistor, R2, is the input impedance determining resistor of this stage and its value 220 Ohms, matches that of the output impedance of the mixer output filter network. It couples the bias voltage generated by the potential divider, R1 and R3, to the transistor's base. The bias chain components can have relatively high values because of the presence of R2. High value resistors would be excluded because of the large thermal noise contributions they would make. However large value resistors are desirable because of their low power consumption. This circuit arrangement has the benefit of a low power consumption, low input impedance and low noise and is described fully in [4.2].

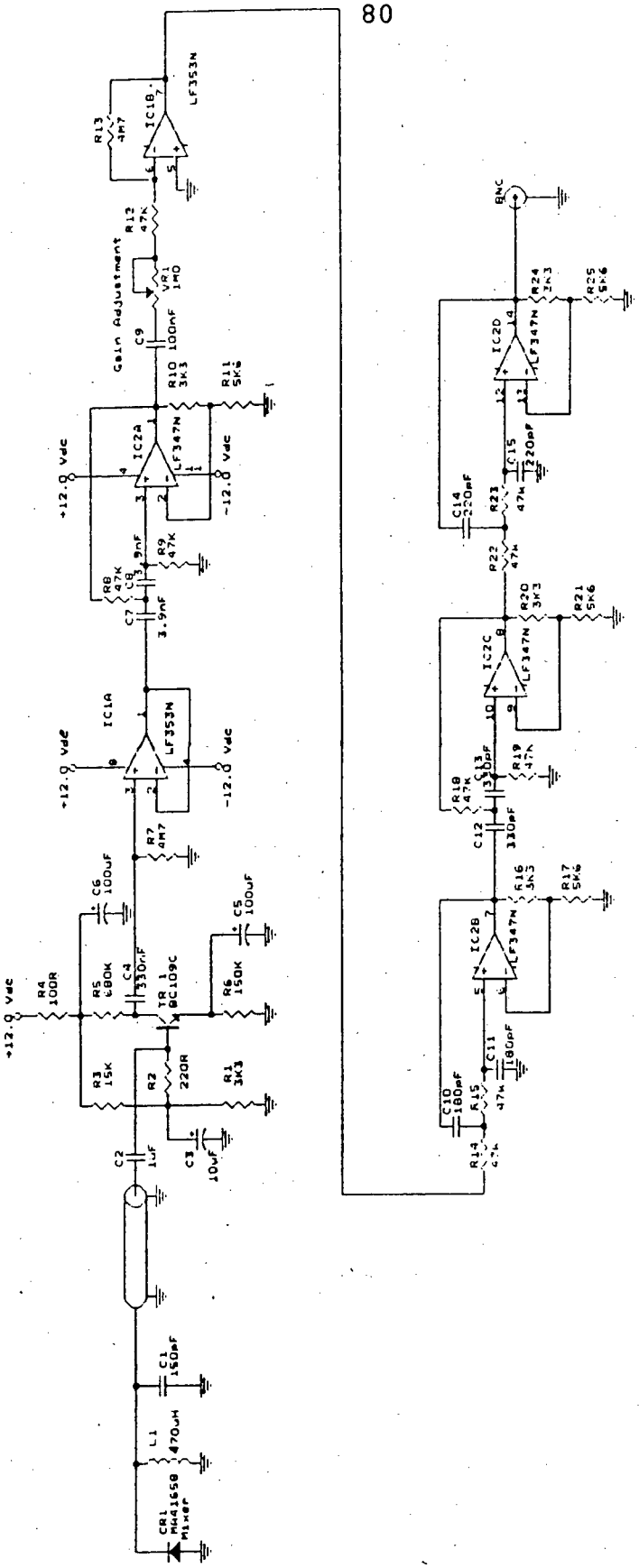

Figure 4.13. Complete circuit schematic of the receiver.

The base voltage of TR1 and it's emitter resistor, R6, determine the emitter/collector current of this stage, which ultimately determines the noise and gain performance. The design equation for this stage is as follows :

$$Ie = \frac{Vb - Vbe}{R6 + (Rb/\beta)}$$

where Vb = Base voltage of TR1,
Vbe = Turn-on voltage of TR1,
Rb = Effective resistance of base bias chain,
β = Current gain of transistor.[4.2]

Therefore $Ie = \frac{+2.16 - 0.6}{(150*10^3 + (2924/350))}$

$= 10.4\ \mu A.$

Capacitor, C5, decouples R6 to ground which has the effect of maximizing this stage's gain without compromising it's DC stability or repeatability. Resistor, R5, is the collector load of TR1 and sets the gain of this stage as well as the DC collector voltage. The gain of this stage can be calculated by the following formula :

$$Av = \frac{(Rc \,//\, Rl)}{(re)}$$

where Rc = Transistor collector load resistor,
Rl = Transistor load resistor,
re = Dynamic resistance of base-emitter junction.[4.2]

$$Av = \frac{(R5 \,//\, R7)}{(0.025/Ie)}$$

$$= \frac{(680*10^{3}//4.7*10^{6})}{(0.025/10.4*10^{-6})}$$

$$= 247.1x = 47.86 \text{ dB.}$$

Capacitor, C6, is the output capacitor which blocks the DC voltage on the collector of TR1 while passing the AC beat frequency signals unattenuated to the buffer stage.

The buffer stage is constructed from half of a LF353N, a device which contains two low noise, wide bandwidth and fast slew rate opamps. IC1(a)'s inverting input is tied to it's output as per the non-inverting unity gain amplifier configuration.

Opamp IC1(a) is connected to ± 12 V DC split regulated power supplies which enable it to have a large unclipped output voltage swing capability. Any clipping would cause spurious harmonics in the output spectrum of the IF beat frequency. The opamp has a high output current drive capability and it effectively isolates the input stage (TR1) from any loading effects due to the subsequent stages.

DC blocking capacitors are used through out the receiver to isolate the stages from each others quiescent DC output voltages. Any long term DC drifting will be amplified by the amplifier chain where it could cause saturation in any one of the stages because of the high gains involved.

Filter Design Procedure.

This method is based on the method described in [4.2]. The filter type is first chosen from Table 4.3. A Butterworth characteristic was chosen as it offers a flat passband, with no peaks in the frequency response or near the cut-off frequency.

Table 4.4.
Filter constants.

n	Type					
	B'worth	Bessel		Chebychev 0.5 dB		Chebychev 2.0 dB	
	K	fn	K	fn	K	fn	K
2	1.586	1.274	1.268	1.231	1.842	0.907	2.114
4	1.152	1.432	1.084	0.597	1.582	0.471	1.924
	2.235	1.606	1.759	1.031	2.660	0.964	2.782
6	1.068	1.607	1.040	0.396	1.537	0.316	1.891
	1.586	1.692	1.364	0.768	2.448	0.730	2.584
	2.483	1.908	2.023	1.011	2.846	0.983	2.904
8	1.038	1.781	1.024	0.297	1.552	0.238	1.879
	1.337	1.835	1.213	0.599	2.379	0.572	2.605
	1.889	1.956	1.593	0.861	2.711	0.842	2.821
	2.610	2.192	2.184	1.006	2.913	0.990	2.946

(reproduced from Horowitz and Hill [4.2]).

The order, n, of the filter is then determined, as this determines the number of active filter stages that are required. If n is even then n/2 filter stages as shown in Figure 4.14 will be needed.

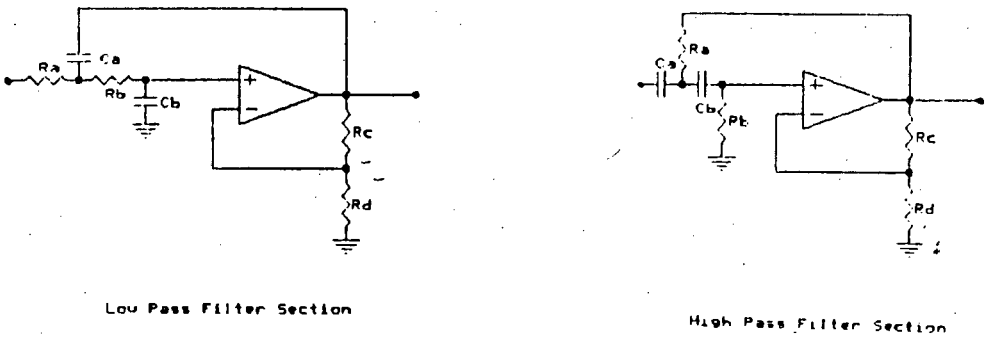

Figure 4.14. Circuit diagrams for the high pass and the low pass filters subsections.[4.2]

For the Butterworth case, within each filter stage, Ra = Rb = Rx, and Ca = Cb = Cx. To determine the values Rx and Cx the following formula is utilised :

$$Rx * Cx = \frac{1}{2*\pi*fc}$$

where fc is the required cutoff frequency (-3dB frequency.)

The final filter components are derived from Table 4.2. The K-factor determines which filter type, ie 2nd order Butterworth case has K = 1.586 which is then used to determine Rc and Rd in Figure 4.14.[4.2]

As an example, the 10 kHz high pass filter will be designed.

Table 4.5.

Filter specifications
fc =10 kHz
2nd Order
Butterworth

Therefore one active high pass filter stage from Figure 4.14 will be required and K is 1.586.

Component values will have to be restricted to E12 values, ie the mantissa of component value will have to be part of the following sequence: 1.0, 1.2, 1.5, 1.8, 2.2, 2.7, 3.3, 3.9, 4.7, 5.6, 6.8, 8.2.

Choosing Rd as 5600 ohms (5k6),

$$Rc = ((K-1)*Rd)$$

$$Rc = (1.586-1)*5k6 = 3k3.$$

and

$$Rx.\ Cx = \frac{1}{(2*\pi*10\ 000)}$$

and

choosing Rx as 47k

therefore

$$Cx = 1/(2*\pi*fc*Rx)$$

$$Cx = 330\ pF$$

$$fc = 10\ 261\ Hz.$$

The resistor values have to be chosen as a compromise, as too large a value results in a high thermal noise contribution, while too low a value results in loading

of the opamp output. The opamp type is unimportant, provided that it has good noise performance, in this case. Referring to Figure 4.13, capacitors C7, C8 and resistors R8 and R9 form the frequency determining network of IC2(a), the first high pass filter with a cut-off frequency of 868 Hz. The gain of this stage, and hence the K-factor, is set by resistors R10 and R11. The opamp is connected to split 12 V DC supplies which endows it with a large output voltage swing capability. The opamp is a quarter section of a LF347N and has the same characteristics as the LF353N as they belong to the same family of devices based on the LF351N single opamp.

Capacitor, C9, prevents any DC from entering the following stage. IC1(b), is configured as an inverting amplifier with a variable gain. The gain of this stage can be determined as shown previously. (See Figure 4.3)

$$\text{Gain, Av} = \frac{-R13}{(VR1 + R12)}$$

therefore

$$\text{Av max} = -\frac{4M7}{47k} = -100x = 40.00 \text{ dB},$$

$$\text{Av min} = \frac{-4M7}{(47k + 1M0)} = -4.49x = 13.04 \text{ dB}.$$

The next filter stage is constructed from IC2(b). The frequency determining network consists of C10, C11, R14 and R15, R16 and R17 set the required K-factor.

This stage is a low pass filter with a cut-off frequency of 18 812 Hz.

The high pass filter which follows this stage has a cut-off frequency 10 261 Hz, it's design procedure was outlined earlier. Filter time constant determining components are C12, C13, R18 and R19, with R20 and R21 setting the gain.

The last filter is a 15 392 Hz low pass filter that has R22, R23, C14 and C15 setting the cut-off frequency. The gain of 1.586 is set by R24 and R25.

The beat frequency output is available at pin 14 of IC2, this is connected to a BNC connector to facilitate connection to oscilloscopes and other test equipment.

Figure 4.15 is the circuit diagram for the filter stages of the receiver, which was entered into a low frequency electronic circuit analysis package called Microcap II™.

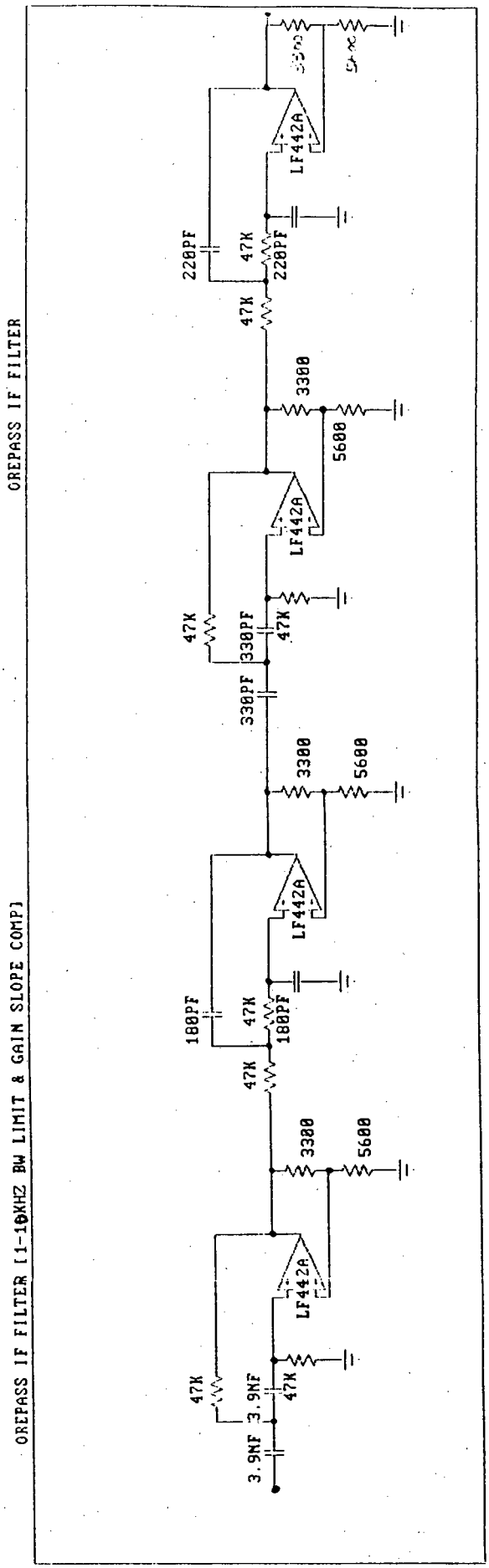

Figure 4.15. Circuit diagram for circuit analysis program.

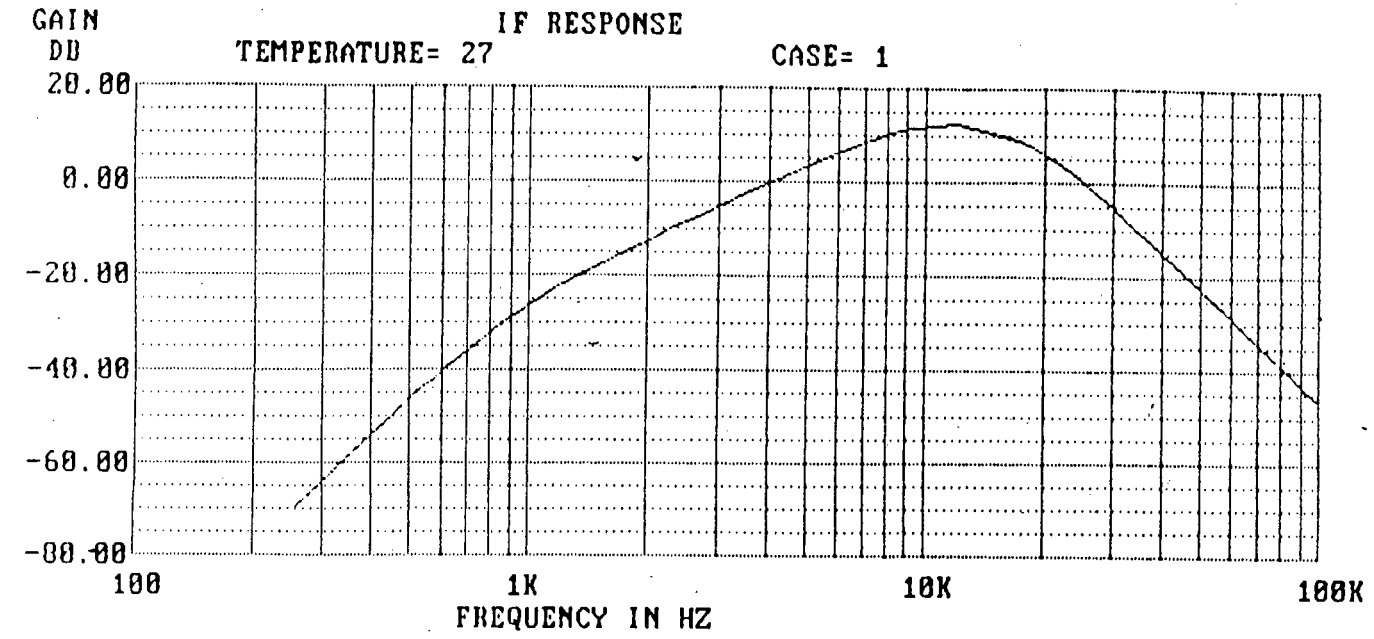

Figure 4.16. Output from circuit analysis package.

Figure 4.16 is the computer predicted frequency response of the filter network, as obtained from Microcap II™. The response shape is precisely that required for this application. The opamps use in the simulation are all LF442A as this is the only FET opamp that the Microcap II™ has in it's library which is closely related to the LF347N. The LF442A is a higher precision version of the LF351N, the base opamp of the whole family.

4.5. The Power Supply.

The mains input to the complete unit is controlled by one switch, SW1, the main on/off switch.

4.5.1. Power supply 1.

The circuit diagram for power supply 1 (PSU1) is shown in Figure 4.17. This unit supplies power to the low power circuitry. Transformer, T2, is rated at 15 Volts AC @ 0.5 Amps, it is center tapped as this supply has dual split voltage outputs.

The bridge rectifier, BR1, is a 1 amp device that converts the AC input into a pulsating DC output. The diodes that constitute the bridge have a maximum peak inverse voltage rating of 100 Volts.

Due to the small power requirements of the circuitry, the main power supply filtering capacitors, C1 to C4, could be rated at 220 uF @ 25 Volts. Two capacitors are paralleled to give an effective capacitor of 440 uF which has a lower height than a single capacitor of 470 uF which is the next closest value available. Because of the lower height of these capacitors, mounting of the circuit boards in the enclosures was facilitated.

IC1 is a 78L12, a low power 12 volt regulator. It regulates the raw DC (approximately +21 V) down to +12 Volts. This forms the main supply for the modulator and the receiver. Capacitors, C3 and C4, are mounted close to the regulator and are for the prevention of regulator instability.

The diode, D1, is provided to protect IC1, during power up and power down, from 'latch-up' which can cause device failure.

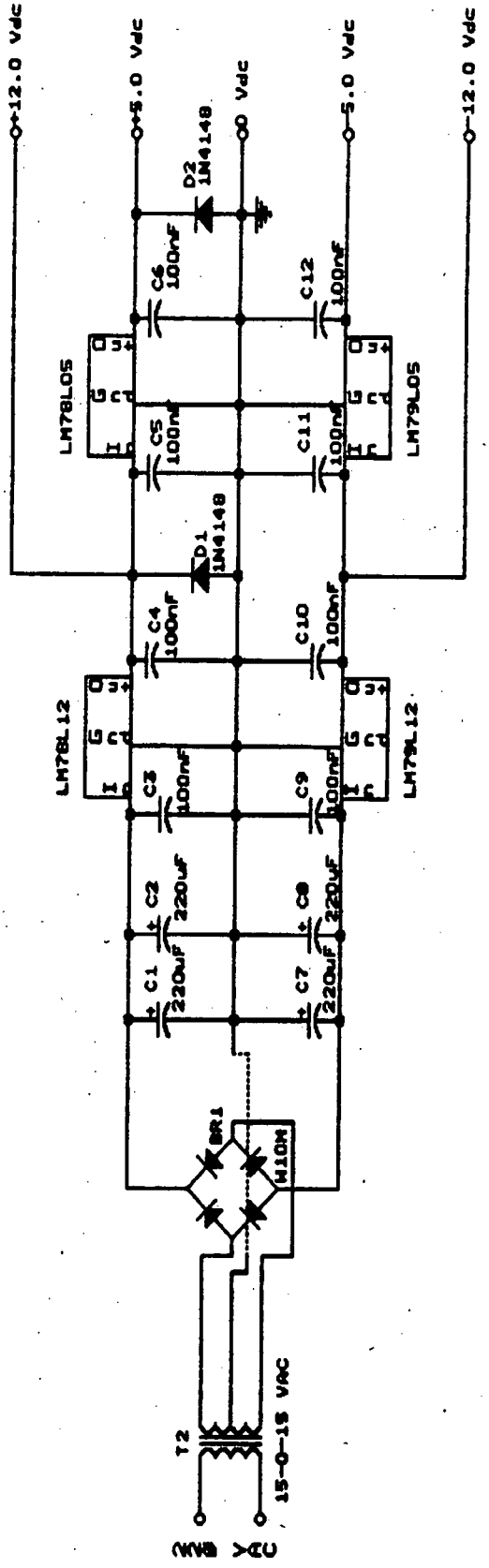

Figure 4.17. Circuit schematic for main power supply.

IC2, a 78L05, regulates the regulated +12 Volts down to +5 Volts for the counter, logic and DAC chips in the modulator.

The stabilisation capacitors for IC2 are C5 and C6, similarly D2 is for the prevention of 'latch-up' in IC2.

The raw negative supply is regulated to -12 volts by IC3, a 79L12, and it is for the opamps in the modulator and receiver. The regulator is stabilised by C9 and C10 which are mounted close to the chip.

The DAC 0800 in the modulator requires a negative 5 Volt supply to operate properly, this is provided by IC4. It is a 79L05 and is stabilised by C11 and C12.

4.5.2. Power supply 2.

It is the high-power power supply that provides the DC bias to the Gunn diode microwave oscillator. The circuit schematic is shown in Figure 4.18.

The mains input is stepped to 12 Volts AC by the transformer, T1, which is rated at 1 Amp.

The low voltage AC is converted to smooth DC by the combination of BR1, the bridge rectifier, and the 4700 uF capacitor, C1.

IC1 is a variable voltage regulator with a maximum current output of 1.5 amps. The output voltage can be adjusted over a wide range depending on the value of the resistors connected to it. In this case the output

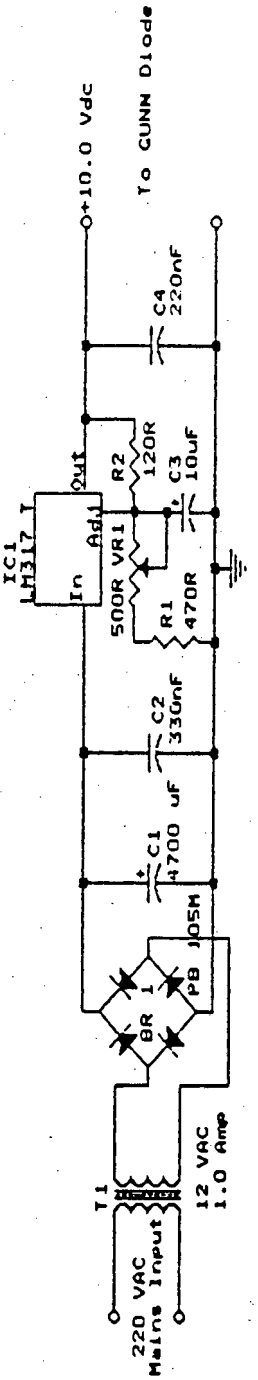

Figure 4.18. Gunn diode power supply circuit schematic.

can be adjusted from 6.45 to 11.35 Volts. The output voltage can be determined by the following formula :

Vout = 1.25 *((VR1 +R1)/R2 +1)

It is adjusted to exactly 10.0 Volts by adjusting VR1. Capacitor, C3, a 10 uF tantalum capacitor is a decoupling capacitor that helps improve the ripple rejection of the chip and it also decreases the noise on the output of the chip.

Capacitors, C2 and C4, are mounted close to IC1 and are the decoupling capacitors that prevent instability of the regulator chip.

4.6. Construction.

The prototype consisted of two enclosures, as can be seen from Fig 3.1, interconnected by means of a multi-conductor cable. The one enclosure housing the bulky power supply components such as the transformers and smoothing capacitors etc. This enclosure also has the ON/OFF switch, power indicator and the Gunn power supply. The other enclosure houses the Gunnplexor™ module, the antenna and the electronics. The cable that connects the two enclosures carries the +10 Volts to the Gunn diode and also carries a 12-0-12 Volts AC signal to the receiver circuitry. The shield of this cable is connected to ground to minimise interference. The separate boxes reduce the possibilty of interactions between the various circuit modules.

The construction of the three prototype circuit boards was undertaken on veroboard, which consists of perforated SRBP board with copper tracks running the

length of the board. Components are mounted by taking their leads through the holes and soldering to the tracks underneath. These tracks, and wire, effect the interconnections between the various components.

This method of construction was favoured over printed circuit boards as it offers a very short developement cycle. Where corrections and modifications are easily effected. However a neat appearance is difficult to achieve and due to the large number of wired interconnections, is not very robust. Although if care is exercised, a reasonably neat and robust result can be achieved. Ultimately the circuits will have to be constructed on printed circuit boards to improve both the reliability and the servicability of the unit. Although the prototype has survived a trip down the mine and back without any ill effects. Two of the three circuit boards are power supply boards while the last one is the modulator/receiver board.

Figure 4.19. Interior view of RX/TX enclosure.

The receiver-modulator power supply (PSU1) is located in the TX/RX (See above.) enclosure to reduce the possiblity interference as much as possible. When the regulators are this close to the circuit board, the chances of power line interference reaching the receiver is very small. The regulators on this board dissipate very little power and hence do not require heatsinking or ventilation. The Gunn PSU (PSU2),see below, with the LM317 regulator chip mounted on a heatsink, is located in the PSU enclosure, as it generates a substantial amount of heat that would be detrimental to the operation of the unit. The modulator/receiver board is mounted as close to the Gunn source as possible to reduce interferece signals. The modulator and receiver although on the same board are displaced by approximately 2 cm from each other. This is to minimise the breakthrough of clock and ramp signals onto the output.

Figure 4.20. Interior view of PSU enclosure.

A grounded aluminium shield is placed below this board as stray coupling occurs between the under board interconnects. The receiver input and output are connected via shielded/coaxial cable to help reduce stray coupling.

The output is available on a BNC connector for easy connection to test equipment ie spectrum analysers etc.

The microwaves are guided out of the enclosure by a section of waveguide that has a special flange that is used to mount the Gunnplexor™ and attach the waveguide to the plastic enclosure. A waveguide matching section is also included on the prototype to match the antenna to the Gunnplexor™. This helps to minimise standing waves in the RF front-end of the receiver which would result in anomalous signals being fed to the digital signal processing unit. The production unit will not have this matching section.

The prototype also has a range filter bypass switch that can be used to switch out the range compensation filter. This is useful to ascertain correct operation of the unit, as well as to determine the location of close-in objects that may be overloading the input stage. It is also helpful in determining if any saturation is occuring in any of the receiver stages.

4.7. References.

[4.1] Clarricoats P., Portable radar for the detection of buried objects, Conference paper 1977.

[4.2] Horowitz, H. and Hill, P. The Art Of Electronics, Cambridge , London, 1985.

[4.3] Motchenbacher C.D. and Fitchen F.C. Low Noise Electronic Design, John Wiley & Sons, USA , 1973.

Chapter 5
SYSTEM ANALYSIS.

5.0. Introduction.

This chapter analyses the system described in the previous chapter as well as looking at the various areas where degradation in performance may be occuring. Possible causes of performance degradation are also investigated.

5.1. The System Parameters.

The beat frequency that the system provides as an output contains all the information about what the system 'sees'. All objects within it's field of view give rise to a frequency component and hence the output signal is highly complex.

In order to calibrate the system, as well as to check whether it is operating correctly requires that the basic output frequency per unit of distance to be calculated.

As the source was assumed linear in chapter 3, when the principle of operation was explained, the varactor bias voltage was set approximately at the center of it's approximately linear tuning range, at 5.50 Volts. The amplitude of the triangle modulation output was set to 3.72 Volts to have a peak to peak frequency deviation of 20 MHz. With an operating frequency of 10.525 GHz. (See Figure 4.4 for tuning characteristic.)

The bandwidth of the IF amplifier was designed as 10 kHz - 1 kHz = 9 kHz, with the intention of low cost.

A full ore pass then should give a beat frequency of 1 kHz while an empty ore pass should give a frequency output of about 10 kHz.

Using equation 3.4,

$$fb = \frac{4*\delta f*fmod*R}{c} \qquad (5.1)$$

and rearranging the subject of the formula,

$$fmod = \frac{fb*c}{4*\delta f*R}. \qquad (5.2)$$

In this case, $\delta f = 20$ Mhz,
$fb = 1$ kHz,
$c = 3 * 10^8$,
$R = 50$ m.

Therefore $$fmod = \frac{1000*3*10^8}{4*20*10^6*50}$$

$$= 75 \text{ Hz}.$$

Rechecking at full range,

$$fmod = \frac{10\ 000*3*10^8}{4*20*10^6*350}$$

$$= 107 \text{ Hz}.$$

Fmod, was set at 80 Hz as a compromise.

Hence $$fb = \frac{4*20*10^6*80*R}{3*10^8}$$

$$= 21.33 * R \qquad (5.3)$$

5.2. Limitations On System Performance.

The limitations of the system can be grouped into two main areas, [5.1] :

i) Factors that impair the accuracy of the unit.
ii) Factors that inhibit the range performance.

5.2.1. Accuracy degradation.

i) Long-term amplitude and frequency drift of the modulation waveform due to thermal heating of the oscillator components. Ageing of the oscillator components can also give rise to similar faults. Amplitude changes will change the frequency deviation of the carrier, δf in above equations will change. Any change in the modulation frequency, fmod in above equations, will also result in a different beat frequency for the same range.

ii) Non-lineararities in the tuning characteristics of the source. These arise because of the non-linear capacitance, see Fig.4.6. Gunnplexor tuning characteristic, change of the varactor diode as the bias voltage is changed. This non-lineararity causes variations in the output beat frequency as the source is swept, with the 'target' at a constant range, which in turn causes a misreading of the range.[5.1]

5.2.2. Range degradation.

The main factor that limits the maximum range that the device can function over is the residual system noise.[5.1 and 5.2]. This noise has many sources, the main contributers will be noted here.

i) Thermal noise, confined to the receiver bandwidth, which is essentially white or has a flat spectral density. The receiver bandwidth is 9 kHz, thermal noise arises from the thermal agitation of electrons within resistances. The open circuit root mean square (RMS) voltage produced by a resistor is given by the following formula :

$$Vt = \sqrt{(4kTBR)} \qquad (5.4)$$

where k = Boltzmann's constant ($1.38*10^{-23}$ Joules/°K),

T = Absolute temperature (°K),

B = Noise bandwidth (Hz),

R = Resistance (Ω).

At room temperature, 4KT = $1.6*10^{-20}$ W/Hz, and B is that of the system that is under consideration. This noise source is also present in all active semi-conducter devices.

Other noise sources include shot noise, which arises from the random diffusion of carriers through the base of a transistor with the random generation and recombination of hole-electron pairs. Contact noise caused by the fluctuating conductivity caused by imperfect contact between any two materials. This is also called 'excess

noise' and 'flicker noise' and is dependant on the DC current flowing through the device.[5.3].

ii) Noise from the Gunn source, any noise that is within the bandwidth, B, from the instantaneous carrier frequency results in a noise output at the IF output. Any small frequency drift about the current operating frequency (ie a small amount of FM) will also result in a noise output at the IF output, this is commonly known as 'phase noise'. These noise contaminations are effectively down converted by the mixing process to the IF output where they contaminate the beat frequency signal.[5.1].

iii) Amplitude modulation, due to the Gunn oscillator output fluctuating as it is swept across δf. This generates noise components at the modulation frequency and its harmonics which manifest themselves in the IF output. Filtering the the IF output, low pass filtering, helps reduce their effects. These signals have a much larger output at the mixer than the return signal from the ore. Hence the first stage of the receiver has to have the dynamic range to cope with these signals. Clipping in the first stage will result in the generation of spurious harmonics at the final output. Therefore the front-end gain cannot be as high as would be preferable.[5.1].

iv) Imperfect isolation and mismatching of the various microwave interconnections gives rise to multiple reflections of signals. These can also reduce the maximum available power output. Broadband matching is difficult to achieve in

practise, problems arise due to the swept source. A mismatched load/antenna can cause tuning characteristic ripples that will not be observed when the source is checked on a standard load, which will not easliy be compensated for even with a EPROM mapped modulator.[5.1]

v) Other noise sources, not covered in i), power supply regulator noise, noise from other electronic equipment and radio frequency interference.[5.1].

vi) Image noise from the mixer. This results from the mixing process where the wanted signal and its image are converted to the image frequency. While there is no signal at the image frequency, there is noise present. This effectively doubles the noise power, resulting in a degradation of the SNR by 3 dB.

vii) Clock breakthrough and noise pickup on the modulation waveform. This will cause spurious frequency modulation of the microwave carrier that will effectively 'smear' the output spectrum of the IF amplifier.

viii) Direct contamination of signals from the modulator to the receiver. The modulator waveform is digitally generated, these signals have a large bandwidth and fast rise-times that are difficult to prevent from interfering with the sensitive receiver circuitry.

All noise sources contribute to the system noise floor which ultimately limits the smallest signal that can be detected. The performance of the system can marginally be improved by

careful circuit design in critical areas.

5.3. References.

[5.1] SHEFER, J., KLENSCH, R., KAPLAN, G. and JOHNSON, H., Clutter-free radar for cars, (5), *Wirelss World*, 1974, 117-122, 199-202.

[5.2] SKOLNIK, M. Introduction to Radar Systems (2nd ed.). McGraw-Hill Inc., Japan, 1980.

[5.3] OTT, H.W., Noise Reduction Techniques in Electronic Systems., John Wiley & Sons, USA, 1976, 198-213.

Chapter 6
RESULTS, ANALYSIS AND DISCUSSION.

6.0. Introduction.

This chapter deals with the results from tests that were undertaken using the ore pass monitor at different locations and with the two antennae described in Chapter 4.

Independent free-space tests and ore pass tests were undertaken for the reasons outlined in Chapter 2. The references Mk1 refer to the prototype with the 26 dB gain antenna and source 1 while Mk2 refers to the 34 dB gain antenna and source 2 attached to the OPM electronics respectively.

6.1. The Free Space Tests.

These tests were undertaken at the university using the smaller antenna as shown in Figure 3.1.

Figure 6.1. Local test-site [Menzies building].

The first development stage tests were done by pointing the unit out of the laboratory window, which is located three floors from ground level, in the Menzies building. The 'target' is the adjacent Leslie social science building which is located a short distance from the Menzies building. Figure 6.1. shows the test-site where the dish antenna of the ore pass monitor is the dark shadow in the lower half of the photograph.

The output spectrum of the OPM when it is pointing at the Leslie building is shown in Figure 6.2. The large signal peak is the beat signal from the 'target'. The range compensation filter was switched in for these measurements.

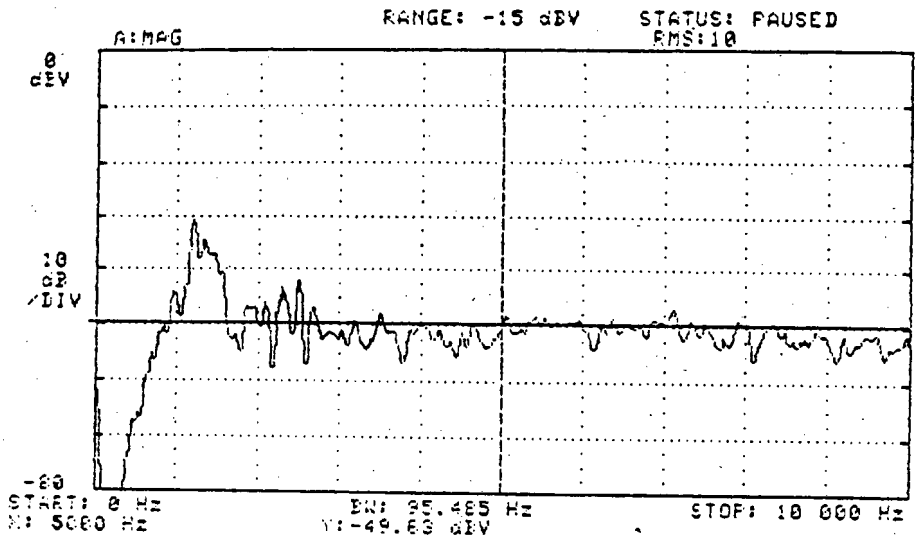

Figure 6.2. Output spectrum of OPM at local test site. [Mk1].

The time domain version of the OPM output is shown in Figure 6.3, together with the linear modulation ramp for the varactor. The range compensation filter was switched out for this measurement as it allows the single return to be easily seen. The range filtered time domain signal is shown

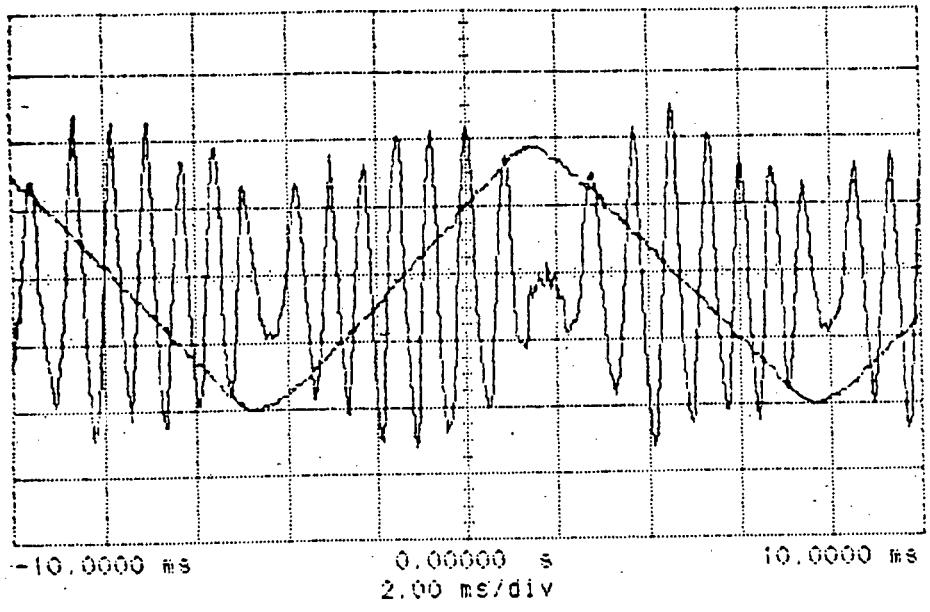

Figure 6.3. Non-range filtered time domain output of OPM at local test site and modulator output. [Mk1].

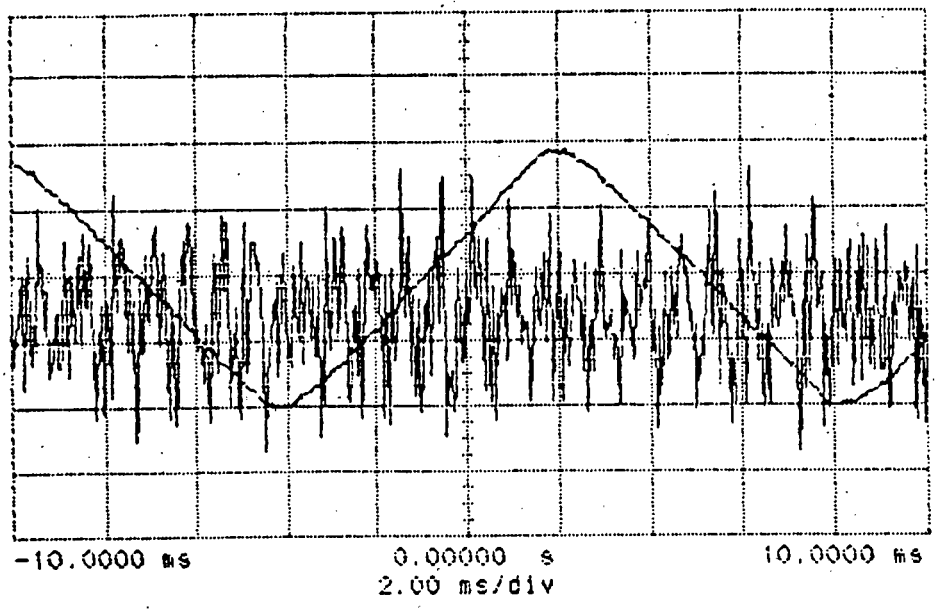

Figure 6.4. Range filtered time domain output of the OPM at the local test site.[No averaging taking place.] [Mk1].

in Figure 6.4., this is the same signal that was shown in

Figure 6.2. It is clearly difficult to see the single return in this signal which is evident in Figure 6.2. One of the benefits of time domain signal averaging is the improvement in the signal to noise ratio as the number of averages is increased. This averaging is achieved by triggering the oscilloscope on the modulation waveform as the beat frequency signal is locked to this waveform. In this way the system essentially performs synchronous detection where the noise gets cancelled to a large extent because of its random nature. This is easily appreciated in Figure 6.5. where the signal that was obscured in Figure 6.4. is visible.

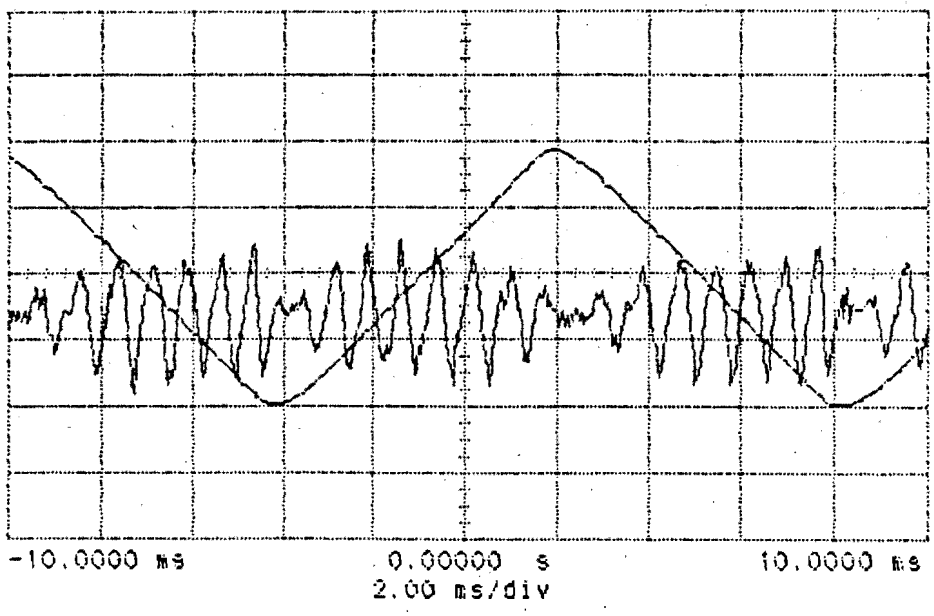

Figure 6.5. Range filtered time domain output of the OPM at the local test site.[Signal averaged 32 times]. [Mk1].

The peak signal, in Figure 6.2., has a frequency of 1200 Hz and an amplitude of ≈-30dBV. Thus the range to the building can be calculated by the calculation outlined in the previous chapter.

$$\text{Range to building} = \frac{3 * fb}{64}$$

$$= \frac{3 * 1200}{64}$$

$$= 3600/64 = 56 \text{ m.}$$

The following set of measurements were taken with the larger antenna but at the same location as the first set. A second more linear source was attached to the antenna for this test and the sweep parameters changed which resulted in a output frequency relationship of 20 Hz/m. The output frequency relationship is more linear as the second source has a better linearity than that of the first source. The results appear in the figures below. The linearity of the source has the effect of making the spectral lines sharper, with less spectral smearing occurring. (Compare Figures 6.2 and 6.6.).

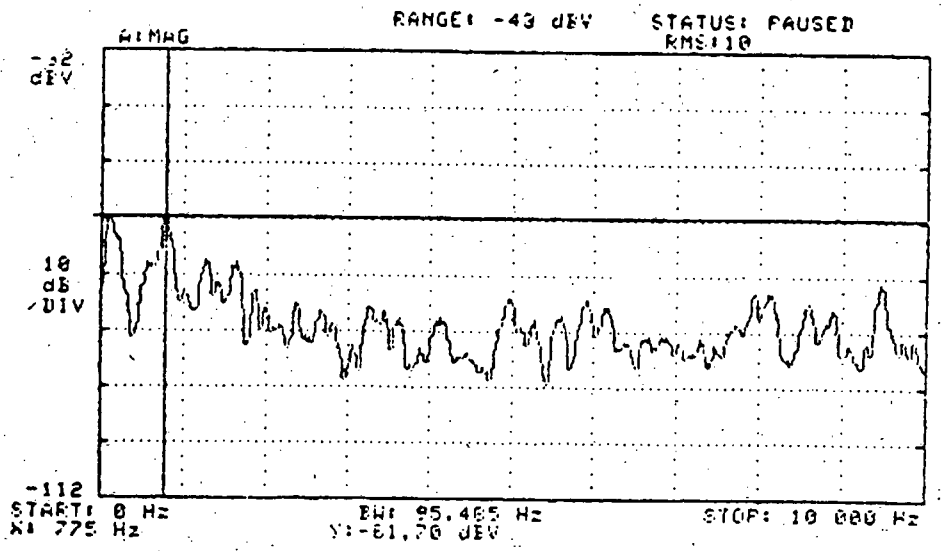

Figure 6.6. Spectrum output of the OPM at local test site. [Mk2].

The peak signal, in Figure 6.6., has a frequency of 775 Hz and an amplitude of -61.7 dBV. Thus the range to the building can be calculated, Range = fb/20 = 775/20 = 39m. The lower-frequency peak is not a radar return but mains break through into the receiver.

The actual distance, measured by means of a plumb line and a measuring tape, is 43 m. Thus the unit measures to the required accuracy of 5m. The error is due to the radar measuring along a line of sight path while the tape measures the ground path-length. The paths are different because of a small rise in the ground level along this path. A corrected measurement would be closer to 41 m, indicating that the unit can measure within 2 m accuracy. The non-linear source of the Mk1 prototype is the cause of the error in the distance measurements between the two prototypes.

Clutter is essentially unwanted reflections from the ground or neighboring buildings or even multiple reflections between the source and the 'target'. If figures 6.2 and 6.6 are compared it is evident that the higher gain antenna has increased this clutter as would be expected from the increased RF gain.

Equipment used for these measurements consisted of the OPM, a HP 3561A signal analyser, a HP 54501A digital storage oscilloscope and a thinkjet printer.

6.2. The Ore Pass Tests.

These measurements were taken down the number one ore pass of the Finsch Mine, in 1989. The level of the ore in each case is indicated by the marker in Figures 6.8 and 6.9. The signal peak is not always as distinct as for the free space tests due to the tests been taken at the maximum range for

the Mk1 prototype. The noise floor of the receiver and spurious sidewall reflections give rise to the base line of the spectrum output, ie 'clutter'.

The ore level was known to be greater that 100 m below the point at which the measurements were taken. Comparing figures 6.9 and 6.2 one sees that although the frequency has increased, due to increased range, the amplitudes are approximately the same i.e. ≈ -30 dBV. Thus the range compensation filter is clearly working as expected.

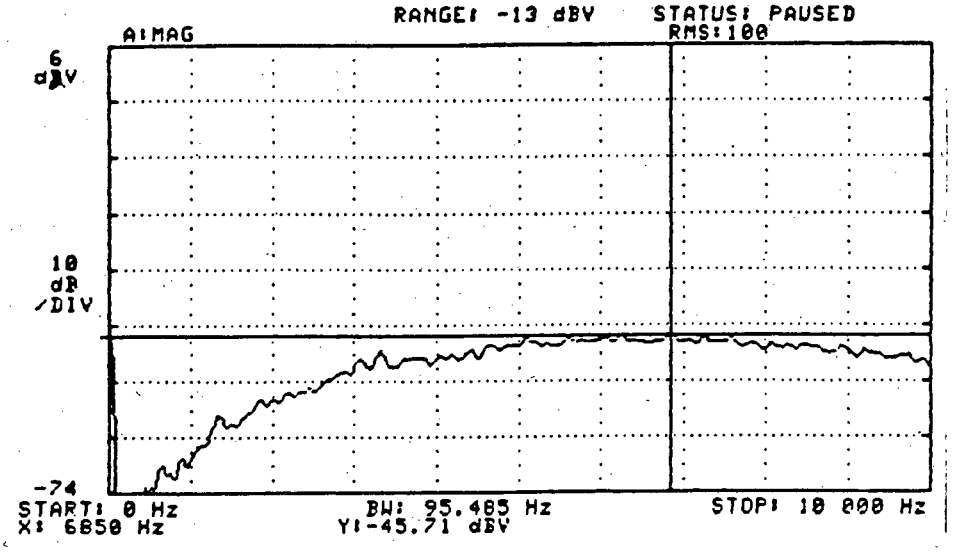

Figure 6.7. Output spectrum of OPM down ore pass.[Using small horn antenna].

Figure 6.7 shows the OPM response when using a small horn antenna of approximately 12 dB gain. No peak is visible in this case as the unit was operating at the limit of its performance. However as ore was added to the ore pass, a peak would become visible depending on how the ore was stacked at the bottom of the ore pass. This test was specifically designed to test operation at the limit of

performance.

There is a reasonably large variation in the amplitude of the return signal as the stacking profile changes, due to the presence of large rocks on top of the ore.

Due to problems with the ore pass emptying apparatus, the full range performance of the unit could not be tested on that particular occasion.

Optimum signal strength is achieved when the OPM is pointing directly downwards. If the orientation is changed so that the beam strikes the side wall, then signal to noise ratio degradation occurs, ie the peak amplitude decreases while the base line stays the same.

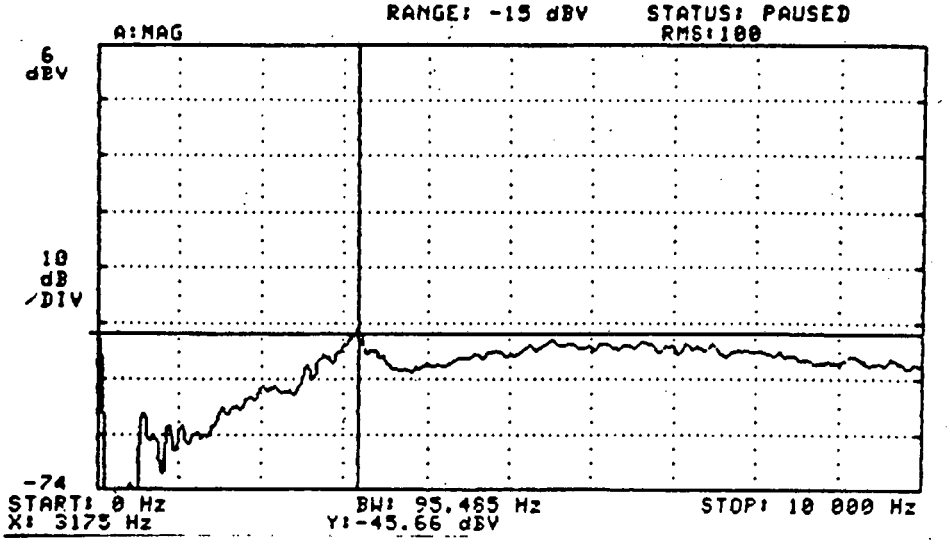

Figure 6.8. Spectrum output from OPM when misaligned down ore pass. [Mk1]

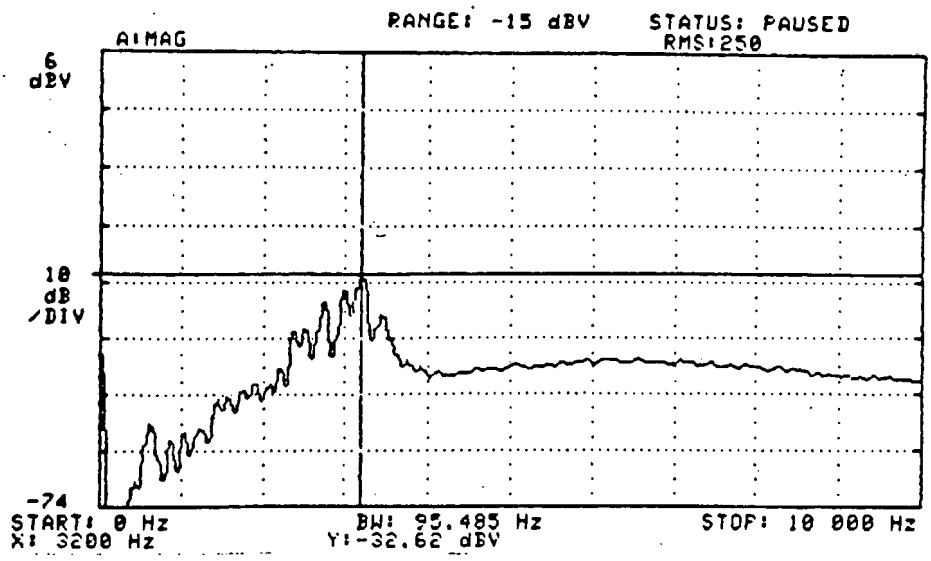

Figure 6.9. Spectrum output of OPM when correctly aligned, down ore pass. [Mk1]

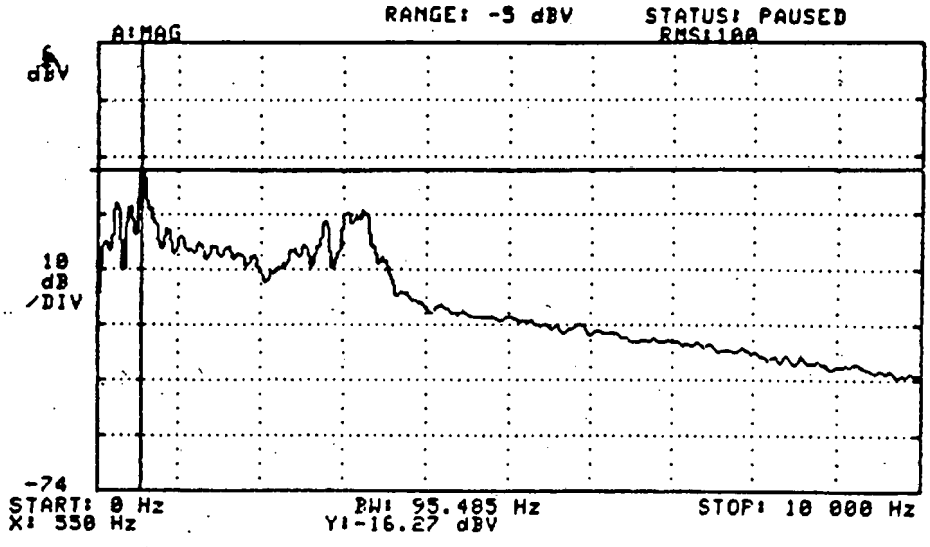

Figure 6.10. Spectrum output of OPM when correctly aligned, with range filter switched out, down ore pass. [Mk1].

Figure 6.8 shows the output of the OPM when it is misaligned. Compared with Figure 6.9, where the unit is optimally aligned, the essential differences are the SNR improvement.

Figure 6.10 shows the spectrum output when no range filtering is applied, the close-in clutter from protruding steel reinforcing rods is clearly visible. This is also evident in Figures 6.8 and 6.9 although to a lesser extent, which is the purpose of the range filter.

The Mk2 prototype was tested down the ore pass and yielded the following results, frequency : 2500 Hz with an amplitude of -35 dBv.

Range = fb/20 = 2500/20 = 125 m.

The increase in signal strength is partly due to the range filter and partly due to the improved reflection from a pool of water on top of the ore. This has the effect of increasing the radar cross-section considerably and hence the amplitude of the return signal.

Chapter 7
FUTURE WORK AND RECOMMENDATIONS.

7.0. System Completion.

The system described earlier only gives an output that is an indication of the depth of ore in the ore pass. Interpretation of this signal is still required as well as conversion into a digital serial data stream and a current loop output suitable for the surface control computers.

There are numerous techniques which can be used to analyse the beat frequency output. The simplest of these is to count the number of zero crossings in one second and thereby calculate the frequency. Another is to use reciprocal timing where the time between zero crossings, the period, is measured. Then by inverting this figure, the frequency can be determined. Genuine spectral analysis of the input signal can be done. Two of the most common techniques used are swept source analysis were a tunable souce is mixed with the input signal and by observing the filtered and rectified mixer output, the spectral composition of the input signal can be found. The other is by direct computation, using a microprocessor, where the input is first sampled, then the Fourier transform applied to this data to give the spectral composition of the signal. A resident microprocessor will also allow the use of sophisticated digital signal processing algorithms[7.1] using a microprocessor controlled frequency counter.

The beat signal is however a complex one as it does not consist of the single frequency indicating the level of the ore but of a wide spectrum that contains reflections from all discontinuities within the ore pass.ie clutter.

The signal analyser is required to cope with dynamics as ore is continually added and withdrawn from the ore pass. A microprocessor supervisor will be the best option available as it will allow for easy communication between itself and the surface computers via the industry standard, RS-232 C. A standard for relatively long digital serial data links. All major microprocessor manufacturers have serial communication chips (USARTS) within their chip sets because of the standard's popularity.

When ore is tipped into the ore pass, it will be in effect a large close-in object that recedes as time passes as it falls down the ore pass. As it is a moving target, the return signal from it will be Doppler shifted. In chapter 3, the beat frequency for triangular modulation and a stationary target was shown in Fig.3.5. The beat frequency for a moving target is shown in Fig.7.1. Where the beat frequency is shifted upwards during the up sweep of the modulator and shifted down during the down sweep.

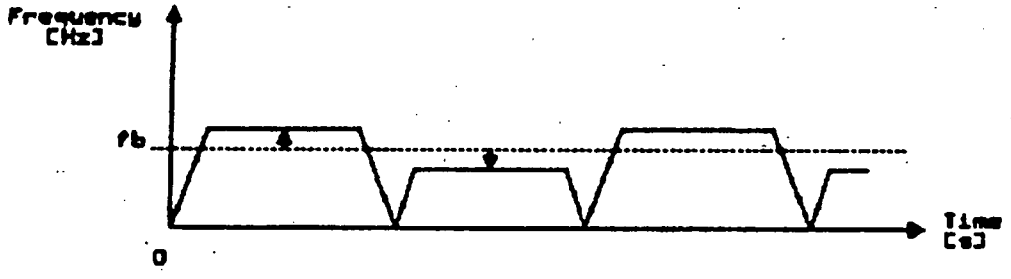

Figure 7.1. Doppler shifted beat frequency.

When the signal of Fig.3.5. is viewed on a spectrum analyser, the single stationary target will appear as in Fig.7.2(a). If it moves then the peak will split in two and the two peaks will then move away from each other. In the case of ore dropped into the ore pass, the ore will at first

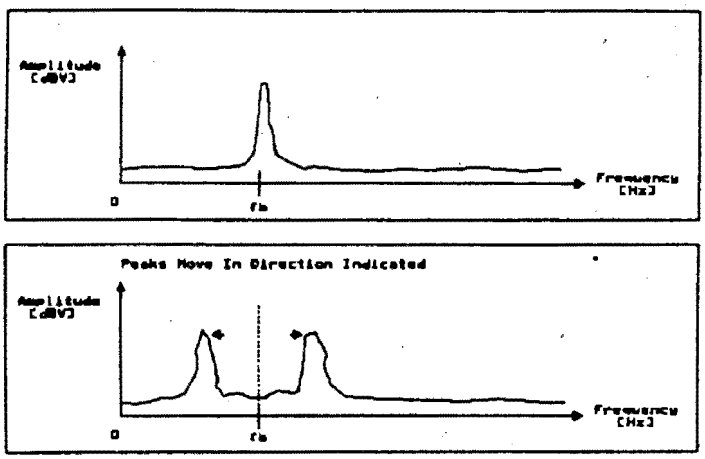

Figure 7.2. Idealised spectrum analyser output for (a) stationary target, (b) moving target.

have an initial downward velocity of zero and then accelerate under the action of gravity. Therefore the peak will split into two and spread apart further and further as the ore gains momentum until impact with the ore at the bottom of the ore pass.

The microprocessor can be programmed to recognise the above conditions and instead of sending rapidly varying ore levels it could send the last stable reading that it had taken to the surface computers. In other words, a software version of the sample and hold hardware function could be implemented. The changing ore profile at the bottom of the ore pass can also give rise to spurious signals which can be ignored if the unit has onboard intelligence.

Another benefit of having a microprocessor onboard is that it will allow the signal analyser to locked onto the beat frequency waveform by synchronising the sampling of the beat signal with the direction line of the counters in the modulator. By doing this the signal analyser can ignore the

spurious signals that occur during the change over period of the modulation waveform.

However, the choice does depend on the availability of support hardware and software as well as access to a specialised development system for the chosen device.

The actual microprocessor chosen for the task is relatively unimportant, provided that it is sufficiently fast enough to calculate the depth of the signal once every 20 seconds.

To convert the time-sampled data signal into it's equivalent frequency domain data requires the computation of it's Fourier transform. The direct Fourier calculation is a lengthy one, the Fast Fourier Transform (FFT) was developed to reduce the time needed for this calculation. It is a computationally more efficient calculation that makes use of the redundancy of information contained within the sampled data.

However general purpose microprocessors are not in general suited to DSP applications. Normal microprocessors are suited to industrial control applications, where the bandwidths are less than 1kHz. This has lead to the development of dedicated signal processing chips which are optimised for these mathematical operations, and where results are required at a semi-realtime update rate. The Texas TMS 32010 and the National DSP 56000 are examples of this. Using a chip of this type will significantly reduce the time required for the FFT calculation as a TMS 32010 can do a single 512 point FFT in 36 ms.[7.2]. A 512 point FFT is neccessary as the FFT output has 256 redundant points. The resolution specification requires 256 discrete frequency points, hence a 512 point FFT is required. However it will still require the presence of a host microprocessor to undertake the tasks of communication, range calculation and

fault recognition. It requires a special development system for the software development.

Another possibility would be the use of a ruggedised version of the popular IBM PC or PC on a card as it is referred to. This solution has very many benefits such as access to high level languages and a vast array of existing add-on hardware cards (A to D, D to A, Realtime Clocks, Digital Signal Processing cards and Serial communications etc.). Cost is a major consideration as it is only available as an imported item and local support in terms of repairs is minimal.

The option which is chosen to complete the project, then essentially depends on the availability of local support and development aids. The options shown above all possess the ability to perform the task although there may be other more cost effective options available.

7.1. Recommendations and Improvements.

The antenna must be replaced by the larger, higher gain antenna to achieve the range performance. (See appendix-c for details of Mk2 antenna.)

The power supply for the Gunn Diode oscillator can be replaced by a lower noise version to lower the noise output of the microwave source.

The filters of the receiver can have their resistor values optimised for lower noise output in the receiver.

Lower noise opamps for the buffer, variable gain stage and the filters can be used again to lower the noise output of the receiver.

The difference between the noise floor of the receiver when the Gunn is 'off'and when the Gunn is 'on' is ≈10 dB. Therefore a large noise contribution is coming from either the Gunn diode or the mixer diode. It is most probably phase noise from the Gunn diode (5.2.2.(ii)), which is a small variation of the carrier frequency about its operating frequency. The amplitude of phase noise falls off rapidly as the observation bandwidth around the carrier increases. Therefore the closer the IF bandwidth (B) is located to DC, the higher the noise power will be in that bandwidth. Then by moving B higher up the frequency scale and observing the noise power, the noise source can be determined. Practically the test would be to increase the modulation rate thereby transposing the beat frequencies to a higher frequency band and developing a new LNA/filter stage for this new band. Measuring the noise floor with the source 'on' and 'off' and comparing to the previous value of ≈10 dB would give an indication of the noise source. Where a reduction would indicate phase noise and no reduction would indicate some other noise source.

Add the EPROM map to linearise the source and allow a wider deviation to be used which should improve the spectral output for a single target. (See appendix-b for the procedure to follow to linearise a source.).(See appendix-a for the circuit schematic of an improved modulator.)

Shield the receiver from the other modules via a special enclosure or a ground plane on the circuit board.

Improve the mechanical construction make it more rugged, use a metal case to lower the suceptability of the unit to outside interference. Include a mains filter to lower mains borne interference.

7.2. References.

[7.1] DELAUDER, D., BALANIS, C. and KAZORSKY, G. Microcomputer based Signal Processor for Short Range F.M. Radar, *Trans. IEEE, IM-35*, 1986, 71-77.

[7.2] MARTIN, N.C, A Microwave Doppler Technique for Vehicle Speed Determination, M.Sc.dissertation of the University of Cape Town. 1987.

Chapter 8
CONCLUSIONS.

This dissertation deals with the problem of measuring the distance down a vertical ore pass as required by the Finsch mine.

A review of the types of radiowave propagation down tunnels was made with relevance to the problem. The final conclusion resulting from tests undertaken in a small tunnel, down the ore pass and the literature was that propagation down the ore pass would be essentially the same as over the same distance in free-space.

A proposed solution of a microwave FMCW radar was offered and a practical system built to prove its viability.

From the various tests the system parameters could be acertained. The critical design features/areas were found to be the RF parameters consisting of the microwave output power, the receiver sensitivity and the antenna gain. Matching between microwave components is crucial but this was a minor concern as the RF front end is a complete bought out unit. Of the receiver eletronics, the front end performance, the minimum detectable signal, is crucial to the whole system's performance. The other circuitry that defines the bandwidth should have it's noise performance minimised. The accuracy of the unit is totally dependant on the modulation waveform's accuracy and stability as well as the varactor tuning characteristic. The linearity of the instrument is critically dependant on the linearity of the source.

Two prototypes were built and tested both in free-space and down the ore pass. They were successful in determining the range to the required accuracy. The accuracy of the one

prototype was marred by it's source's non-linear tuning characteristic.

System completion requires the addition of a signal processing unit of which a microprocessor based unit would be the best suited for the application when the communication and calculation requirements are considered.

It has been shown that the proposed instrument for measuring the depth of ore in an ore pass by the FMCW radar principle works to the required accuracy. It is concluded that the instrument has commercial viability and a place in the mining industry.

BIBLIOGRAPHY.

BYDAL, R., HURLBUT, K. and MORI, T. High Resolution Instrumentation Radar. *Trans. IEEE, IM-36*, (1), 1986, 110-114

CHIBA, J. and KATSUHIKO, S. Effects of Trains on Cutoff Frequency and Field in Rectangular Tunnel as Waveguide., *TRANS. IEEE, MTT-30*, (5), 1982, 757-759

CLARRICOATS, P. Portable Radar For The Detection Of Buried Objects., Radar Conference Paper 1977.

CRAVEN, G., KNIGHT, V and KARBOWIAK, A. Waveguide for long-distance communication. (A swept frequency method for automatic recording of waveguide attenuation.), *PROC. IEE, Vol. 110*, (1), 1963, 71-76

DELAUDER, D., BALANIS, C. and KAZOVSKY, L. Microcomputer Based Siganl processor For Short Range FM Radar., *TRANS. IEEE, IM-35*, (1), 1986, 70-77.

GLAZIER, E. Transmission and Propagation (1st. ed.)., Her Majesty's Stationery Office, London, 1958, 150-179

JACARD, B. and MALDONADO, O. Microwave Modelling of Rectangular Tunnels., *TRANS. IEEE, MTT-32*, (6), 1984, 576-581

JONES, M.H. A Practical Introduction To Electronic Circuits (2nd. ed.)., Cambridge University Press, Cambridge, 1985

LATHI, B.P. Modern Digital and Analog Communication Systems. (1st. ed.), Holt Saunders, Japan, 1983, 285-339.

APPENDICES

Appendix A
New Modulator.

This new modulator has been designed to improve the performance of the OPM. It has a number of new features namely that it is crystal controlled thereby ensuring the stability of the modulation waveform. It's EPROM map allows the storage of any waveform that can be used to linearise any source. A synchronising output is available to enable a signal analyser to synchronised to the sweep voltage thereby allowing time-domain averaging to be applied. A special digital to analogue converter chip has been used that has laser trimmed resistors to ensure the stability and accuracy of the D to A conversion process.

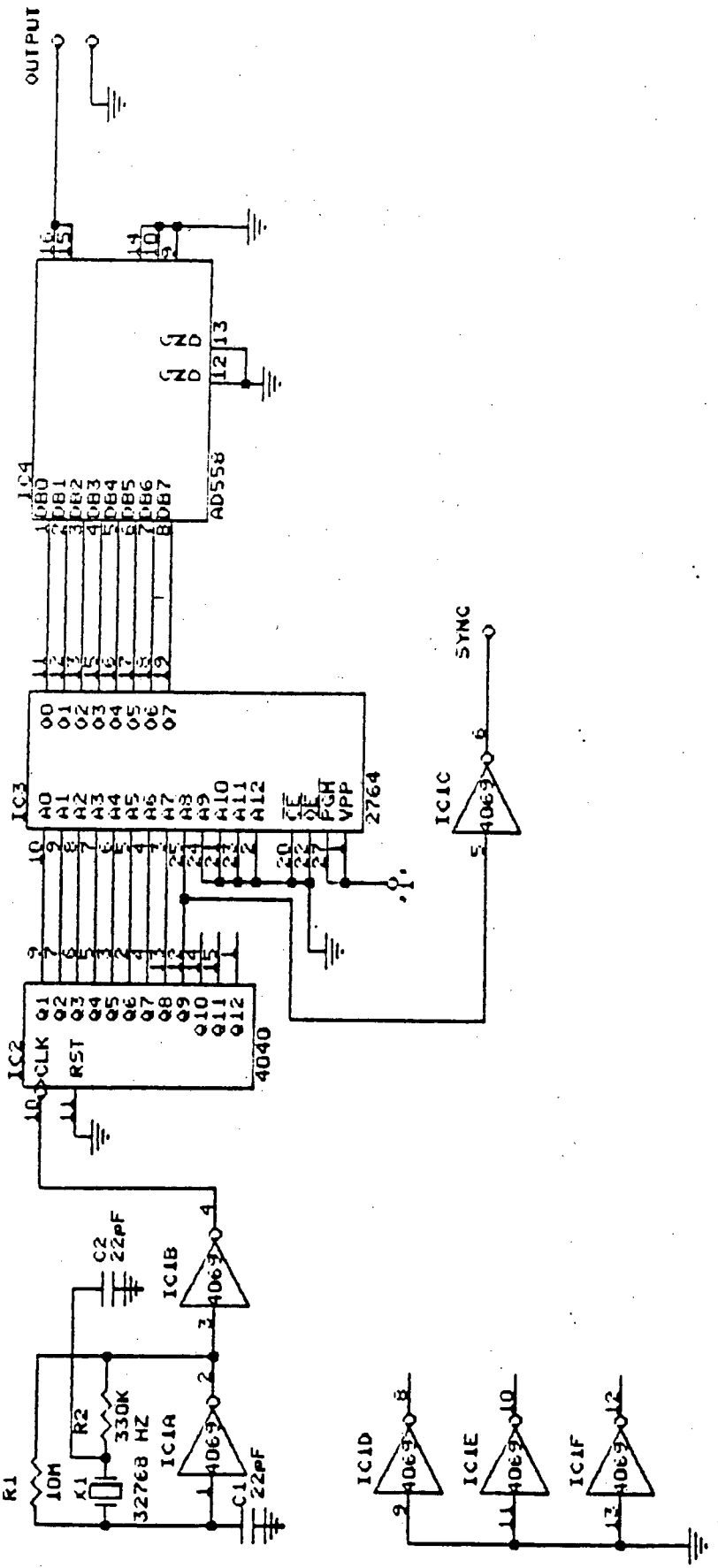

Figure A-1 Circuit schematic for improved modulator.

Appendix B
Source Linearisation Method.

The hardware configuration shown in Figure B-1 can be used to accomplish the linearisation of the source. The specifications of the linear source will be a linear sweep from 10.28 GHz to 10.30 GHz in 256 discrete steps. The Gunn diode needs a regulated DC bias of +10.0 VDC.

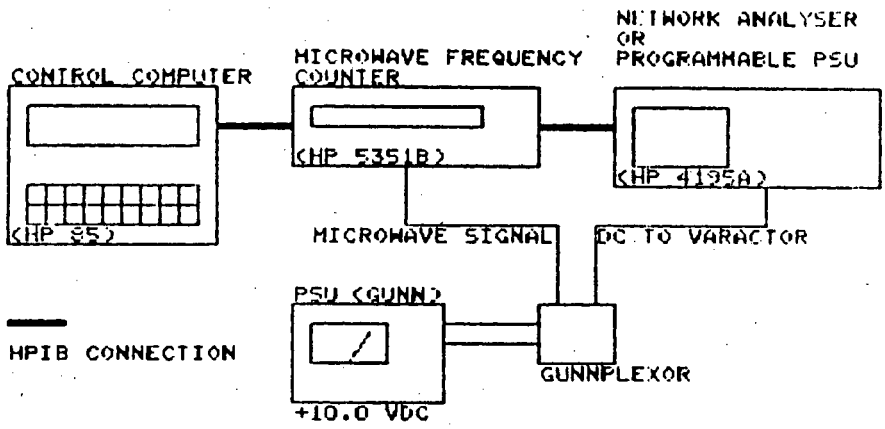

Figure B-1 Hardware configuration for source linearisation.

1) All pieces of equipment must be connected and must be switched on before the power is applied to the Gunn diode. Proceed to step 2.

2) The complete tuning characteristic of the device under test (DUT) is obtained by stepping through all of the 256

voltages that will be available from the D to A in this modulator. The frequency and voltages are stored in an array in the computer for later use. Proceed to step 3.

3) A stability test is performed on the DUT to ascertain is the DUT has reached thermal equilibruim. This is achieved by checking the start frequency again and comparing it to the value stored in the computer's array. If the frequencies are the same then proceed to step 4) else got back to step 2).

4) The start and stop frequencies of 10.28 and 10.30 GHz are found from the computers's memory to check if DUT is compatible. If not the source is rejected ie disconnect this source, reconnect another and goto step 1.). If the source is compatible then proceed to step 5.

5) All the 256 frequencies from 10.28 to 10.30 GHz inclusive together with their corresponding varactor voltages are obtained from the computer's memory and stored in another array. There will be a certain amount of repication of data in this array as there are 256 steps in a much smaller interval. This array now contains the required data for the EPROM. These voltages are now output individually to the varactor and the source frequency measured to complete the stability and linearity test. Proceed to step 6).

6) This data is now displayed in HEX format first according to increasing array index and then in decreasing array index to achieve a linear triangular modulation of the Gunn frequency.

Figure B-2 below contains a map for a linearised source, displayed in HEX format. A listing that performs the source linearisation software in HP 85 BASIC is shown in Figure B-3.

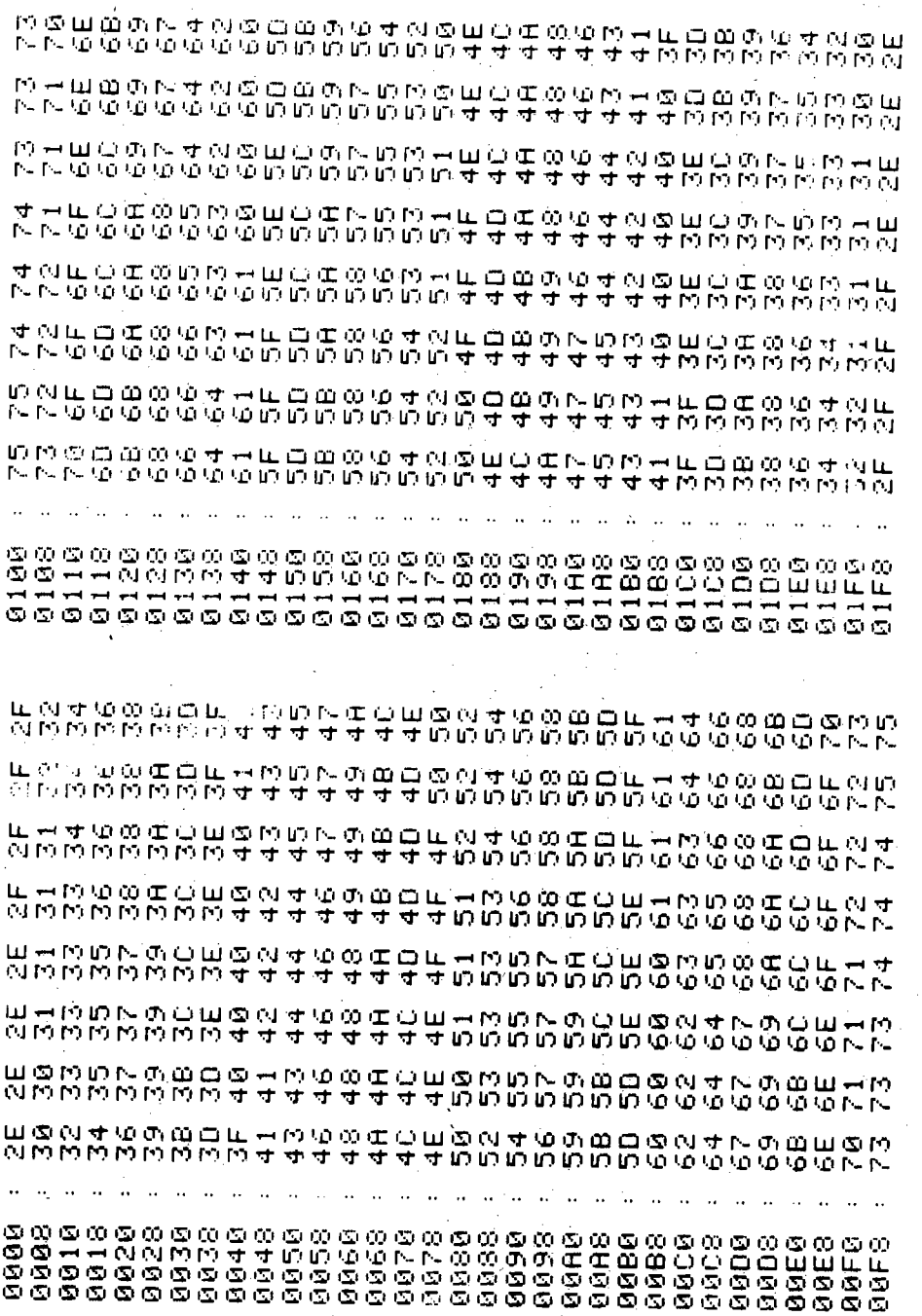

Figure B-2 HEX map for linearised Gunnplexor Source.

Appendix C
Antenna and housing construction diagram.